Perspectives on continental rifting processes from spatiotemporal patterns of faulting and magmatism in the Rio Grande rift, USA

Alyssa L. Abbey[1,2], Nathan A. Niemi[1]

[1]*Department of Earth and Environmental Sciences, University of Michigan, Ann Arbor, MI USA*

[2]*Now at Department of Earth and Planetary Science, University of California, & Berkeley Geochronology Center, 2455 Ridge Road, Berkeley, CA, USA*

KEY POINTS

1) Initiation of the Rio Grande rift appears to be synchronous ~25 Ma and does not support a northward propagation model

2) Extension is accommodated by faulting in the northern and southern Rio Grande rift and by magmatic injection in the central Rio Grande rift

3) Different rift accommodation mechanisms may be controlled by pre-existing weaknesses and lithospheric properties (i.e. thickness)

ABSTRACT

Analysis of spatiotemporal patterns of faulting and magmatism in the Rio Grande rift (RGR) in New Mexico and Colorado, USA yields insights into continental rift processes, extension accommodation mechanisms, and rift evolution models. We combine new apatite (U-Th-Sm)/He and zircon (U-Th)/He thermochronometric data with previously published thermochronometric data to assess the timing of fault initiation, magnitudes of fault exhumation, and growth and linkage patterns of rift faults. Thermal history modeling of these data reveals contemporaneous rift initiation at ca. 25 Ma in both the northern and southern RGR with continued fault initiation, growth, and linkage progressing from ca. 25 Ma to ca. 15 Ma. The central RGR, however, shows no evidence of Cenozoic fault-related exhumation as observed with thermochronometry and instead reveals extension accommodated through Late Cenozoic magmatic injection. Furthermore, faulting in the northern and southern RGR occurs along an approximately north-south strike, whereas magmatism in the central RGR occurs along the northeast to southwest trending Jemez lineament. Differences in deformation orientation and rift accommodation along strike appear to be related to crustal and lithospheric properties, suggesting that rift structure and geometry are at least partly controlled by inherited lithospheric-scale architecture. We propose an evolutionary model for the RGR that involves initiation of fault-accommodated extension by oblique strain followed by block rotation of the Colorado Plateau, where extension in the RGR is accommodated by faulting (southern and northern RGR) and magmatism (central RGR). This study highlights different processes related to initiation, geometry, extension accommodation and overall development of continental rifts.

PLAIN LANGUAGE SUMMARY

We identify patterns of faulting and volcanism in the Rio Grande rift (RGR) in the western US to better understand how continental rifts evolve. Using methods for documenting rock cooling ages (thermochronology) we determined that rifting began around 25 million years ago in both the northern and southern RGR. Rift faults continued to develop and grow for another 10 to 15 million years. The central RGR, however, shows that rift extension occurred through volcanic activity both as eruptions at the surface and as magma injection below the surface since ~15 million years ago. Interestingly, RGR faulting in the north and south parts of the rift occurs on a north-south line while volcanism in the central RGR is along a northeast to southwest line. The

differences in the location and orientation of faulting and volcanic activity may be related to the thickness of the lithosphere beneath different parts of the rift. Using these patterns of faulting and magmatism we propose the RGR evolved through a combination of oblique strain--extension diagonal to the rift, and block rotation--where the Colorado Plateau is the rotating block. This detailed study highlights different processes related to the accommodation of extension and the overall development of continental rifts.

1. INTRODUCTION

Continental rifting may eventually lead to tectonic plate break-up, an essential part of the tectonic cycle, and yet, the processes that accompany rift initiation, define rift geometry or fault style, control the location of extension, and govern differences in rift extension accommodation mechanisms remain unclear (Nelson et al., 1992). Ultimately, continental rifting is caused by interactions between mantle flow and plate movements; accordingly, extension accommodation, rates of rift development, and fault growth are controlled by combinations of heat transfer, lithospheric structure, far-field stresses, mantle flow, and magmatism (Lavecchia et al., 2017). Additionally, the mechanisms that accommodate extension may be controlled by crustal and lithospheric properties such as strength, thickness, pre-existing weakness, inherited structure, and composition and/or rates of extension (e.g. Buck, 1991; Brun, 1999; Corti, 2012; Fletcher et al., 2018). As such there are numerous expressions of rifting, for example, rifts can be wide, narrow, magma dominated, have large basin-bounding faults, numerous intra-basin faults, or en echelon geometries (e.g. Ebinger 1984; Ebinger 1989; Nelson et al., 1992; McClay et al., 2002; Molnar et al., 2017; Brune et al., 2017), emphasizing the roles that faulting and magmatism can have on the geometry and extension accommodation of a rift system

(Fig. 1; e.g. Buck, 2004; Ebinger, 2005; Buck, 2006; Corti, 2009).

Continental rift systems grow initially as separate basins dominated by the initiation and linkage of individual fault segments (e.g. Morley, 1988; Morley et al., 1990; Nelson et al., 1992; Contreras et al., 2000; McClay et al., 2002; Ebinger, 2005; Corti, 2008; Abbey and Niemi, 2018). Continued growth of separate rift basins via fault tip propagation and segment linkage leads to these basins merging and connecting with each other through what are generically termed *accommodation zones* (e.g. Morley, 1988; Ebinger 1989; Morley et al., 1990; Nelson et al., 1992; Chapin and Cather, 1994; Lewis and Baldridge; 1994; Mack and Seager, 1995; McClay et al., 2002). Such accommodation zones (ACZs) promote basin integration through strain transfer between and across faults, often facilitating magmatic activity that further aids in strain transferal (e.g. Lewis and Baldridge, 1994; Rowland et al., 2010; Muirhead et al., 2015; Muirhead et al., 2016).

Understanding the spatiotemporal relationships between faulting and magmatism will assist in distinguishing between processes of rift development (e.g. basin growth and linkage and/or hot spot migration; Fig. 1) and controls on rift geometry and extension accommodation (e.g. inherited structure or lithospheric architecture). These new insights about rift initiation and development will be helpful for determining the processes and factors controlling the evolution of continental rift systems around the world where there is less available data or more limited access.

Rift initiation and fault growth style (e.g. tip propagation, segment linkage, or constant length with increasing displacement; Kim and Sanderson, 2005) can be well documented is the Rio Grande rift (RGR) in the western United States (Fig. 2). The entire rift system is exposed on land, and a plethora of published data related to fault motion, basin sedimentation, volcanism, lithospheric structure, and regional strain rates provides a thorough framework necessary for establishing relationships between faulting, magmatism and lithospheric structure (Table 1). Moreover, extension in the RGR is relatively slow (Woodward, 1977; Golombek et al., 1983; Savage et al., 1990; Shirvell et al., 2009; Kreemer et al., 2010; Muirhead et al., 2016; Nixon et al., 2016; van Wijk et al., 2018; Liu et al., 2019), which affords the opportunity to capture discrete details about fault growth and rift basin linkage that might otherwise be difficult to detect in more developed rifts and/or more rapidly evolving extensional systems (e.g. Ethiopian rift, Gulf of California).

Here we review existing interpretations and controversies about the evolution of the Rio Grande rift and summarize the physiographic characteristics, which have influenced many of the contradicting explanations about RGR development. We then synthesize all of the published low-temperature thermochronometry data available along the RGR to elucidate spatial patterns of rift-flank fault initiation, growth, and linkage (Figs. 3, 4, and 5). Supplementing these data we present new thermochronometric samples and analyses designed to constrain the total magnitude of rift-related extension (typically ZHe) or to refine the uncertainty on the initiation of faulting (typically AHe) (Table 2). Using inverse thermal history modeling on these data assembled into vertical transects (combining the compiled published data with our new data) we obtain initiation timing, and magnitudes and rates of exhumation along the rift-flank faults of the RGR. Finally, we assess compositional and spatiotemporal patterns in magmatism to further identify and constrain processes of rift basin linkage and extension accommodation.

2. RIO GRANDE RIFT CONTROVERSY

Aspects related to the temporal growth of the RGR are highly disputed, with debate centering around two main hypotheses.

(1) Extension began in the southern part of the rift and propagated northward over time so that the basins in the northern RGR are the youngest in the rift system (McMillan et al., 2002; Leonard, 2002; Heller et al., 2003; Frankel and Pazzaglia, 2006; Duller et al., 2012). Rift growth via propagation gains support from general models involving propagating faults that connect through pre-existing weak zones or migration of magma. Within the RGR, far field tilting of Miocene sediments, increased sedimentation in the Great Plains, and the existence of young (<6 Ma) mafic volcanism and seismic activity in northern Colorado have been invoked as evidence for a northward propagation model (McMillan et al., 2002; Leonard 2002; Heller et al., 2003; Duller et al., 2012; Kellogg, 1999; Naeser et al., 2002; Leonard et al., 2002; Cosca et al., 2014; Nakai et al., 2017).

(2) Rifting was primarily synchronous along the length of the RGR (Chapin and Cather, 1994; Landman and Flowers, 2013; Ricketts et al., 2016). Typical models supporting synchronous rifting include either block rotation or oblique strain (Fig 1; Ebinger 1984; Brown and Golombek, 1986; Ebinger, 1989; Nelson et al., 1992; McClay et al., 2002; Kreemer et al., 2010; Busby et al., 2013; Molnar et al., 2017; Lavecchia et al., 2017; Brune et al., 2017). Additionally, inter-basin syn-rift sedimentation and thermochronometry data from the rift flanks have been invoked to support a model of synchronous rift

initiation (Chapin and Cather, 1994; Ingersoll, 2001; Landman and Flowers 2013; Ricketts et al., 2015). However, syn-rift strata, and basin subsidence in individual basins of the RGR often have poor age resolution (van Alstine and Lewis, 1960; van Alstine, 1969; Baldridge et al., 1994; Zhu and Fan, 2018; van Wijk et al., 2018) and rift-related magmatism is sparse in many RGR basins (McMillan et al., 2000; Cosca et al., 2014). Additionally, regional tilting or distal erosion and sedimentation are indirect proxies for rift activity, hampered by a deficiency of coherent detail along the entire length of the rift and potentially being ascribable to non-tectonic processes (e.g. climate; van Wijk et al., 2018). Therefore, we lack a set of criteria by which we can reliably distinguish between rift models proposed for the development of the entire RGR system.

2.1. Approach to resolving spatial and temporal patters of faulting and magmatism in the Rio Grande Rift

Fault segment growth and linkage can be observed and quantified with low-temperature thermochronometry analyses in vertical transects collected on exhuming normal fault blocks (Stockli et al., 2000; Stockli et al., 2002; Curry et al., 2016; Abbey and Niemi, 2018; Boone et al., 2019). Low-temperature thermochronometers are powerful tools for understanding near-surface (1-7 km) thermal histories of the crust and thus are sensitive to processes that affect the upper crust, including erosion and faulting. Low-temperature thermochronometry can be used throughout the RGR to constrain timing, rates, and magnitudes of faulting as these approaches are sensitive to temperature ranges from ~30 °C to ~230 °C depending on mineral system and radiation damage—

apatite (U-Th-Sm)/He (AHe): ~30 and 90 °C; apatite fission track (AFT): ~70 and 150 °C; zircon (U-Th)/He (ZHe): ~130 to ~230 °C (Kelley and Chapin, 1995; Farley, 2002; Reiners et al., 2002; Reiners, 2005; Ehlers, 2005; Shuster et al., 2006; Flowers et al., 2009; Guenthner et al., 2013).

We compile AHe, ZHe, and AFT data from 15 studies amounting to over 400 low-temperature thermochronometry ages that span >800 km along-strike of the RGR (Table 1; Figs. 3, 4, and 5). We analyze the spatial distribution of these data and extract sample suites which we consider to have spatial relationships consistent with a vertical sampling transect. We define a vertical transect as including at least three thermochronometric samples that are within 5 km of the fault trace at the surface. We targeted places where >500 m was traversed in vertical space across <5 km of horizontal space to ensure a high-relief relationship between the samples. We identified one to four groups of samples that fit our criteria for a vertical transect in each RGR basin with the exception of the three southern-most basins, (Palomas, Jornada and Tularosa basins) where there were no such spatial relationships in the published samples (Figs. 3, 4, and 5; Table 3).

In total we identified 14 groups of samples which fit our criteria for a vertical transect (Figs. 3, 4, and 5; Table 3). Many of these transects are comprised of samples from multiple studies while in other cases samples may have been originally collected in a vertical transect but had not previously been modelled as such. Applying modern thermal history modeling techniques to these newly-compiled vertical transects, we develop a consistent approach to identifying the onset of faulting within the RGR.

Rift initiation has also historically been identified by the onset of voluminous volcanism or eruption of specific magmatic compositions, namely mafic or bi-modal volcanism (e.g. Bailey, 1974; Tweto, 1979; Johnson and Thompson, 1991; Kellogg, 1999; Cosca et al., 2014; Ricketts et al., 2015), although recent studies from the East African rift imply that volcanism cannot necessarily be used as a proxy for rift activity (e.g. Corti et al., 2019). Therefore, we assemble published data on Cenozoic volcanic rocks in Colorado and New Mexico to summarize and evaluate spatial, temporal, and compositional patterns in magmatism and compare the spatiotemporal patterns of rift-related volcanism to the fault initiation and exhumation patterns determined from the thermochronometry data.

2.2. Physiography of the Rio Grande rift

Physiographic characteristics (e.g. narrow or wide grabens, asymmetric or symmetric faulting, voluminous volcanism versus lack of magmatism, and/or changes in graben trend/strike) within continental rifts are partially attributed to differences in extensional accommodation mechanisms, which in rift systems, can be either faulting, magmatism, or a combination of the two (e.g. Buck, 2004; Reyners et al., 2007; Ebinger et al., 2013; Muirhead et al., 2016; Molnar et al., 2017; Lavecchia et al., 2017). The Rio Grande rift (RGR) is a >1000-km-long continental rift that extends from potentially as far south as the Big Bend area on the Texas-Mexico Border (e.g. Muehlberger et al., 1978; Nakai et al., 2017; van Wijk et al., 2018), through New Mexico to central Colorado (Fig. 2; Kelley et al., 1992; Knepper, 1974; Limbach, 1975), and possibly as far north as southern Wyoming, USA (e.g. Kellogg, 1999; Naeser et al., 2002; Leonard et al., 2002; Cosca et al., 2014; Nakai et al., 2017). The majority of the basins formed from RGR extension are asymmetric half grabens (Kellogg, 1999) with significant exhumation occurring along north-south striking basin-bounding normal fault systems connected by various accommodation zones (Figs. 2 and 6; Lewis and Baldridge, 1994; Kellogg, 1999; Naeser et al., 2002; Ricketts et al., 2016). The surface expression of the RGR varies from north to south, displaying distinct physiographic differences (Ingersoll, 2001). The southern RGR is composed of several wide asymmetric grabens at a given latitude, each basin is bounded by a single north-south striking normal fault, and this region has minor Quaternary volcanism. The central RGR is bound by northeast-southwest striking left-lateral strike-slip faults. There are also numerous north-south striking intra-basin normal faults with little vertical offset, and voluminous Miocene to Quaternary volcanism. The northern RGR is characterized by narrow asymmetric grabens bounded by a single north-south striking normal fault at a given latitude and is nearly entirely devoid of rift-related volcanism. Such remarkable differences in the surface expression of rifting lead us to question whether or not the physiography of the RGR might provide insight into the development and evolution of the RGR and emphasize the need to explore patterns of both faulting and magmatism holistically along the entire rift system.

3. SUMMARY OF THERMOCHRONOMETRY, MAGMATISM AND EXTENSION IN THE RIO GRANDE RIFT

Because we are interested in determining information about both the timing of rift initiation and about rift extension accommodation mechanisms, we summarize faulting and magmatism information from each RGR basin below. We focus on low-temperature thermochronometry datasets, which provide details on fault growth, and spatiotemporal relationships in magmatism, which offer insight into extension accommodation via dike injection rather than normal faulting. We acknowledge that basin sedimentation is another useful proxy for information on basin development and rift timing, however, because syn-rift sedimentation is not well dated throughout the entire RGR and is not necessarily helpful in distinguishing between accommodation mechanisms we do not go into those details in the text and instead include published information about basin sedimentation timing, source, and thicknesses in Table 1.

3.1. Southern Rio Grande rift

The southern RGR exhibits the greatest amounts of horizontal extension in any section of the rift, with 50% extension accommodated by several grabens at a given latitude (i.e. the Palomas, Jornada, and Tularosa basins; Chapin and Cather, 1994; Fig. 3). The individual basins range in size from ~20-50 km wide and ~80-150 km long. The faults bounding these basins are north-south striking high angle (>60° dips) normal faults.

Published low-temperature thermochronometry data from the basin-bounding ranges include minimal AFT and AHe data showing early Cenozoic ages in the mountain ranges not bound by active faults and Miocene cooling ages in the mountain ranges uplifted by active extensional faults (Table 1; Fig. 3; Kelley and Chapin, 1997; Ricketts et al., 2016).

Late Cenozoic volcanism within the southern RGR is sparse, represented by several minor Quaternary basalt flows (the Jornada del Muerto, Carrizozo, and Potrillo volcanic fields; Fig. 6; McMillan et al., 2000; NM Bureau of Geology and Mineral Resources, 2003). To the west of the three southern-most basins are the mid-Cenozoic Mogollon-Datil ignimbrites, which are attributed to slab retreat and slowing plate convergence rates at the end of the Laramide Orogeny and are assumed to predate the onset of RGR extension (Fig. 6; McMillan et al., 2000; Chapin et al., 2004).

The northernmost basin in the southern RGR is the southern Albuquerque Basin, which we define as the area from south of Socorro, NM to Albuquerque, NM (Figs. 2 and 3). It is the widest of any of the individual rift basins in the RGR spanning ~80 km from east to west and has undergone ~28% extension (Chapin and Cather, 1994; Russell and Snelson, 1994). This basin contains numerous high angle (>70-80°) faults along several small mountain ranges (Fig. 3; Table 1; Machette, 1988; Ricketts et al., 2015).

Low-temperature thermochronometry data from these mountains show that the western side of the basin is dominated by Oligocene to Miocene cooling ages, whereas the eastern side of the southern Albuquerque Basin preserves Paleocene to Oligocene cooling ages (Table 1; Fig. 3; Kelley et al., 1992; Ricketts et al., 2015; Ricketts et al., 2016). At the base of the Magdalena Mountains we collected a sample for ZHe analysis and obtained a cooling age of 14.4 ± 0.6 Ma (Tables 2, 3 and S1; Fig. 3).

Although there are several low-volume extrusive deposits in the southern Albuquerque Basin, there is no significant rift-related volcanism. However, the southern Albuquerque Basin is known to be underlain by the Socorro magma body, at a depth of ~19 km and comprising an area of ~3400 km^2. This magma body is the cause for much of the present-day seismicity in central New Mexico (Sanford et al., 1977; Balch et al., 1997; Nakai et al., 2017).

3.2 Central Rio Grande rift

The central RGR encompasses a transition from rift-extension dominated by large basin-bounding normal faults and minor magmatism to a section controlled by strike-slip faulting, minor intra-basin faults and voluminous volcanism (Figs. 4 and 7; Koning et al., 2016; Grauch et al., 2017). The central RGR includes the northern Albuquerque Basin (Albuquerque, NM to Santa Fe, NM) and the Española Basin (Kelley, 1979; Fig. 4). The style of faulting in the central RGR is significantly different from that in the southern RGR. The central RGR is bound by two northeast-southwest striking left-lateral strike-slip faults; the Embudo fault, which has accommodated left-lateral slip since ~12-11 Ma (Kelson et al., 2004; Koning et al., 2016; Grauch et al., 2017), although, it also has a significant amount of normal motion to the south (Brown and Golombek, 1986; Liu et al., 2019), and the Tijeras fault (Fig. 4). In addition to these large strike-slip faults, the Sandia Mountains have been uplifted on the east side of the northern Albuquerque Basin by several normal faults, most prominently, the high-angle Rincon fault and tilted Knife Edge fault (Kelley and Duncan, 1986, Machette et al., 1998; House et al., 2003; Ricketts et al., 2015; Table 1; Fig. 4). Both the northern Albuquerque and Española basins are characterized by a distributed set of north-south striking intra-basin normal faults (~10-20 km long), which accommodate minimal vertical offset (Fig. 4; Machette et al., 1998; Grauch et al., 2017; Liu et al., 2019). Horizontal extension in the northern Albuquerque Basin is 17% (Chapin and Cather, 1994) and no known extension estimates are available for the Española Basin.

Low-temperature thermochronometry data from the central RGR reveals Miocene cooling on the east side of the northern Albuquerque Basin (Table 1; Fig. 4; Kelley and Duncan, 1986; House et al., 2003), but cooling ages range from the late Cretaceous to the Eocene surrounding the Española Basin (Table 1; Fig. 4; Kelley and Duncan, 1986; Kelley et al., 1992; Ricketts et al 2016). We collected a sample at the base of the Santa Fe

Mountains for AHe analysis, which yielded a cooling age of 58.7 ± 3.6 Ma (Tables 2, 3 and S1; Fig. 4).

Late Cenozoic (<10 Ma) volcanism in the central RGR is voluminous, with compositions ranging from felsic to mafic (Figs. 6 and 7). The spatial extent of this young volcanism is not confined to the rift boundaries but extends along a northeast-southwest trend from Arizona to Kansas, following the Jemez Lineament (Fig. 6; e.g. NM Bureau of Geology and Mineral Resources, 2003; Chapin et al., 2004; Grauch et al., 2017).

3.3 Northern Rio Grande rift

The northern RGR is relatively narrow in comparison to the basins of the southern and central RGR and is composed of three en echelon grabens (from south to north, the San Luis, upper Arkansas River, and Blue River grabens), each bounded by a single normal fault, forming an asymmetric half-graben (Fig. 5). The three basins range from 5 km to 75 km wide and 60 km to 200 km in length, with high angle (>60°) north-south striking normal faults producing high-relief mountains along the basin flanks (Figs. 2 and 5; Miller, 1999; U.S. Geological Survey, 2006; Landman and Flowers, 2013; Morgan, 2017; Abbey and Niemi, 2018). The basin bounding faults in the northern RGR are hypothesized to be re-activated Laramide structures (Tweto, 1979; Ingersoll, 2001; Liu et al., 2019). Extension estimates in the northern RGR are 8-12% in the San Luis Basin (Kluth and Schaftenaar, 1994; Chapin and Cather, 1994) with no estimates published for the upper Arkansas River or Blue River basins. The basins in the northern RGR have little internal deformation (Kluth and Schaftenaar, 1994) although there is a central horst

(Alamosa Horst) in the middle of the San Luis Basin that causes the deepest parts of the basin to be on the flanks (Brister and Gries, 1994; Kluth and Schaftenaar, 1994).

Low-temperature thermochronometry cooling ages in the footwalls of the normal faults that define the northern RGR grabens reveal that fault exhumation initiated in the Oligocene, continued to at least the late Miocene and that in some places exhumation continued into the Quaternary (upper Arkansas River Basin; Table 1; Fig. 5; Cunningham, 1977; Bryant and Naeser, 1980; Lindsey et al., 1983; Lindsey et al., 1986; Kelley and Duncan, 1986; Shannon, 1988; Kelley et al., 1992; Naeser et al., 2002; Landman and Flowers, 2013; Ricketts et al., 2016; Abbey and Niemi, 2018). In contrast to the relatively young cooling ages on the faulted sides of the northern RGR half grabens, cooling ages on the passive sides of these grabens are substantially older, ranging from Cretaceous to Eocene (Naeser et al., 2002; Landman and Flowers, 2013; Abbey et al., 2017; Fig. 5).

New AHe ages from the base of the southern and northern Sangre de Cristo Mountains are 8.8 ± 0.5 Ma and 7.4 ± 0.5 Ma, respectively, and a new ZHe age from the base of the central Sangre de Cristo Mountains is 19.4 ± 0.4 Ma (Tables 2, 3 and S1; Fig. 5).

Rift-related volcanism in the northern RGR basins is essentially non-existent, with the exception of the Miocene-aged Taos Plateau volcanic field blanketing the basin fill in the southernmost part of the San Luis Basin (Fig. 6). On the west and east margins of the rift respectively are the expansive Eocene-Oligocene San Juan and Thirty-nine Mile volcanic fields, which, as with the Mogollon-Datil volcanic field in southern New Mexico, are interpreted to be related to flat-slab-subduction and roll-back at the end of the Laramide orogeny (Chapin et al., 2004). Sparse volcanic deposits with rift-related chemical signatures and ages (<6 Ma) exist about 50 km west of the northernmost rift basin (Blue River Basin) in the northern RGR (Fig. 6; Leat et al., 1989; 1990; Cosca et al., 2014). Recent seismicity, along with these volcanic rocks and extensional features (faults) similar in age to rifting (Tweto, 1979), suggest the possibility that the rift extends as far north as Wyoming (Nakai et al., 2017). However, no clearly defined range-bounding normal faults north of those studied here have been identified as targets for low-temperature thermochronometry sampling.

4. RESULTS AND INTERPRETATIONS FROM INVERSE THERMAL HISTORY MODELING OF LOW-TEMPERATURE THERMOCHRONOMETRY DATA

Inverse thermal history modeling provides a way to explore many possible cooling histories for a given sample or group of samples to resolve exhumation histories from low-temperature thermochronometric data. The power of this approach is magnified when samples with varying closure temperatures and/or with known vertical spatial relationships can be jointly inverted to find a cooling history that satisfies the data obtained from all of the samples. The more vertical space covered along the exhumed fault block then the more information can be gleaned about the initiation of fault motion as well as the minimum temperatures to which the rock were exposed at depth.

We use the program QTQt (QTQt64R5.6.2a; Gallagher, 2012) for inverse thermal history modeling of 14 compiled vertical transects comprised of thermochronometry data from 130 samples along the RGR (Figs. 3, 4 and 5; Table 3). QTQt has the ability to incorporate multiple samples with a known spatial relationship (i.e. vertical transects) and can invert for thermal histories from different thermochronometers simultaneously within the same model. A multi-sample modeling approach allows for identification of thermal histories that satisfy the observed data, geologic assumptions, and model constraints, which helps to avoid unjustified structure of a thermal history that can occur when over-fitting data from an individual sample (Gallagher et al., 2005). The outputs from these inverse thermal history models are the ‘most-likely’ time-temperature paths that a sample or group of samples may have undergone (Figs. 3, 4 and 5), which helps to resolve questions related to timing, magnitudes, and rates of exhumation along the faults adjacent to which the samples were collected.

We assume sample location relationships did not change as the rocks were exhumed to the surface and that each sample in the transect has experienced the same exhumation history. However, exhumation along a normal fault implies the footwall samples have experienced some amount of tilting that is related to the dip of the fault (Stockli et al., 2000; Shirvell et al., 2009; Johnstone and Colgan, 2018), which means the paleo-vertical distance between the samples is different from the present-day vertical distance. To account for this difference in paleo versus modern vertical distance between samples, we project the samples from a single transect onto the fault plane on which they were exhumed (Abbey and Niemi, 2018). This projection allows us to determine the fault-parallel distance (i.e. the paleo-vertical distance between the samples) at the time the samples underwent exhumation. These fault-parallel distance relationships are input as pseudo-elevations in our inverse thermal history models (Table 3).

4.1 Fault initiation and exhumation in the Rio Grande rift

4.1.1 Southern Rio Grande rift

The three southernmost RGR basins (Palomas, Jornada, and Tularosa) do not have any thermochronometry samples that fit our criteria for a vertical transect, so we did not perform any inverse thermal history modeling on data from those basins. We note, however, that the cooling ages from the thermochronometric data on the active basin-bounding faults are generally between ~20 Ma and 5 Ma (Fig. 3; Kelley and Chapin, 1997; Ricketts et al., 2016). Although we cannot determine fault initiation timing and rates or magnitudes of exhumation, we can use these data to infer that fault exhumation occurred during the Miocene in the southernmost RGR basins.

4.1.1.1 Southern Albuquerque Basin

Three vertical transects were identified and used for inverse thermal history modeling in the southern Albuquerque Basin (Table 3). The North Baldy transect from the Magdalena Mountains includes AFT data from Kelley et al. (1992) and ZHe data from this study (Table 3) and constrains exhumation on the La Jencia fault, with the earliest onset of faulting at ca. 25 Ma (Fig. 3). Exhumation proceedes from ~25-19 Ma at a rate of ~0.3 mm/yr and increases to ~0.5 mm/yr from ~19-16 Ma. From 16 Ma to present we cannot resolve a specific pulse of cooling; however, fault exhumation continued at an average rate of 0.2 mm/yr (Fig 3). The total magnitude of exhumation recorded from the North Baldy transect is ~7 km (Fig. 3).

The Polvadera Mountain transect, from the Lemitar Mountains, is comprised of AFT data from Kelley et al. (1992) and records exhumation on the Socorro Canyon fault (Table 3; Fig. 3). Fault initiation appears to occur at ~12 Ma, at an exhumation rate of

~0.4 mm/yr until ~8 Ma, at which point the exhumation rate decreases to an average of 0.3 mm/yr from 8-0 Ma (Fig. 3). Total exhumation on this fault segment was >4 km (Fig. 3).

To the north, along the Loma Pelada fault, the Ladron Peak transect includes AFT data from Kelley et al. (1992) and AHe data from Ricketts et al. (2015) (Table 3). Fault initiation occurs at ~14 Ma, exhuming the footwall at a rate of ~0.7 mm/yr from 14 to 11 Ma followed by slower exhumation at an average rate of 0.2-0.3 mm/yr from 11 Ma to present (Fig. 3). The magnitude of exhumation recorded by the Ladrom Peak transect is ~5 km (Fig. 3).

4.1.2 Central Rio Grande rift

4.1.2.1 Northern Albuquerque Basin

We performed inverse thermal history modeling on one group of AFT and AHe samples (Kelley and Duncan, 1986; House et al., 2003) exhumed on the Knife Edge fault at the base of the Sandia Mountains (Table 3; Figs. 4 and 6). This model incorporates a constraint box to account for burial estimates made by House et al. (2003), who suggest that ~2.4 km of section was overlying the Sandia Mountains at the end of the Cretaceous and that another 1-2.5 km was added to that cover during the end of the Laramide Orogeny. Motion along the Knife Edge fault appears to initiate at ~24 Ma, with exhumation proceeding until ~16 Ma at a rate of ~0.4 mm/yr, bringing rock from ~5 km depth to within <1 km of the surface. From ~16 Ma to present there is <1 km of exhumation recorded in the Sandia Mountains (Fig. 4).

4.1.2.2 Española Basin

Thermochronometric ages in and around the Española Basin range from ~80 to ~30 Ma (Fig. 4; Kelley and Duncan, 1986; Kelley et al., 1992; House et al., 2003). Thermal history modeling of the Santa Fe transect with AFT data from Kelley and Duncan (1986) and AHe data from this study shows that all of the samples were close to reasonable surface temperatures by ca. 50 Ma (Table 3; Fig. 4), which suggests that the Nambe Fault at the range front of the Santa Fe Mountains does not accommodate a large enough amount of rift-related vertical fault displacement to detect with low-temperature thermochronometry methods. Thus, the timing of exhumation adjacent to, and in the vicinity of the Española Basin seems to be entirely associated with the Laramide Orogeny in agreement with Baldridge et al. (1994). This places a limit on rift related exhumation of <~1.5 km in the western Santa Fe Mountains.

4.1.3 Northern Rio Grande rift

4.1.3.1 San Luis Basin

In the San Luis Basin, we identified three groups of samples that fit our criteria for a vertical transect (Fig. 5; Table 3). In the southern San Luis Basin, the Wheeler Peak transect includes AFT data from Kelley and Duncan (1986) and AHe data from this study and shows fault exhumation at a rate of ~0.4 mm/yr from 25 to 20 Ma. Post-20 Ma the thermal history modeling does not recover any discrete pulses of cooling, and exhumation occurs at an average rate of 0.2 mm/yr. Overall >6 km of exhumation is recorded by the Wheeler Peak transect (Fig. 5).

In the north-central part of the San Luis Basin, the Sand Dunes transect incorporates AHe, AFT, and ZHe data (Kelley and Duncan, 1986; Ricketts et al., 2016;

and this study; Fig. 5; Table 3) and reveals fault initiation at ~14 Ma at an exhumation rate of ~1.0 mm/yr from 14 to 11 Ma. From 8 Ma to present footwall rocks exhumed from ~4 km depth at a rate of 0.5 mm/yr. This transect records >7 km of exhumation (Fig. 5).

The northernmost vertical transect in the San Luis Basin, the Mount Owens transect, includes AFT and AHe data (Lindsey et al., 1986; and this study; Table 3) as well as a constraint to represent conodont analyses from Lindsey et al. (1986) that indicates burial to temperatures of 200-300°C (Fig. 5). Thermal history modeling shows that from ~25-20 Ma fault exhumation occurred at a rate of 0.4 mm/yr. After 20 Ma the footwall continued to exhume at an average rate of ~0.15-0.2 mm/yr until the present-day, with no discrete pulses or changes in exhumation recovered over this time period. Total exhumation recorded by the Mount Owens transects is >5 km (Fig. 5).

4.1.3.2 Upper Arkansas River Basin

The upper Arkansas River (UAR) Basin has the highest density of published low-temperature thermochronometry data and we identified four transects useful for assessing rift-related exhumation (Table 3). In the south, the Mount Shavano transect includes AHe and AFT data (Shannon, 1988; and Abbey and Niemi, 2018; Table 3) and reveals fault initiation at ~16 Ma, exhuming at a rate of ~0.5 mm/yr until ~12 Ma. After ~12 Ma, exhumation rates slow and discrete cooling pulses are not captured in the model, although exhumation continues at an average rate of <0.2 mm/yr. The Mount Shavano transect records ~4 km of exhumation (Fig. 5).

In the south-central part of the Sawatch Range fault system, the Mount Princeton transect, which includes ZHe, AFT, and AHe data (Kelley et al., 1992; Rickets et al., 2016; and Abbey and Niemi, 2018; Fig. 5; Table 3), records fault initiation at ~24 Ma. Rapid exhumation occurred at a rate of ~0.6 mm/yr until ~19 Ma. A second pulse of exhumation began at ~5 Ma, exhuming rock from to the surface at a rate of ~0.7 mm/yr. This transect records >7 km of exhumation (Fig. 5).

In the northern part of the Sawatch Range, the Mount Belford transect, composed of AHe and ZHe data (Abbey and Niemi, 2018; Table 3), records onset of cooling at ~20 Ma, although no distinct cooling pulses are discernable in the thermal history post-20 Ma. Samples were exhumed a total of ~4 km at an average rate of 0.2 mm/yr from 20 Ma to present (Fig. 5).

The northernmost transect in the UAR Basin that records exhumation is the Mount Elbert transect, composed of AHe and AFT data (Bryant and Naeser, 1980; and Abbey and Niemi, 2018; Table 3). Exhumation on the Mount Elbert transect is observed from ~3 km depth at a rate of ~0.4 mm/yr from ~7 Ma to present (Fig. 5).

4.1.3.3 Blue River Basin

In the Blue River Basin, which is the northernmost asymmetric rift-basin in the RGR, we identified two vertical transects in the southern part of the Gore Range (Table 3). The Buffalo Mountain transect consists of AFT data (Naeser et al., 2002) and reveals heating, possibly by burial at ~14 Ma followed by rapid exhumation from ~4 km depth at a rate of ~0.5 mm/yr beginning ~10 Ma and slowing to a rate of ~0.3-0.4 mm/yr from 7 Ma to the present (Fig. 5).

The Keller Mountain transect includes AHe and AFT data (Naeser et al., 2002; and Landman and Flowers, 2013; Table 3) and chronicles exhumation from 18 to 15 Ma at a rate of ~1.3 mm/yr. The thermal history model also uncovers a pulse of exhumation from 2-0 Ma at a rate of ~1.0 mm/yr. The total magnitude of exhumation recorded by the Keller Mountain transect is >6 km (Fig. 5).

4.3 Summary of low-temperature thermochronometry data and inverse modeling

In the southern RGR fault initiation occurs at ca. 25 Ma on at least one fault segment (North Baldy transect). Other fault segments in the southern RGR record rapid exhumation occurring at different times and rates, with faults typically being active for several million years at a time, starting between 20 and 12 Ma and continuing to the present (Fig. 3). In the central RGR, the majority of the cooling recorded is prior to rift initiation, with the exception of the southern-most transect (Sandia Mountains), which records fault initiation at ca. 25 Ma (Fig. 4). In the northern RGR, numerous fault segments initiate at ca. 25 Ma, however, other individual fault segments progressively initiate over the following 10 m.y., and several fault segments show a renewed exhumation pulse post-5 Ma (Fig. 5).

In summary, there are fault segments within the RGR that initiated at ca. 25 Ma throughout the entire rift. Exhumation rates during the early phase of faulting are higher in the northern RGR (~0.4 to 0.6 mm/yr), compared to the southern RGR (~0.3 mm/yr; Figs. 3 and 5). Fault initiation, growth and linkage appears to be a progressive process in the RGR, with additional fault segments initiating throughout the middle Miocene. This progressive, and protracted, onset of faulting is consistent with high-density thermochronometric studies (Abbey and Niemi, 2018), as well as with detailed structural studies (Liu et al., 2019) in northern RGR. As additional fault segments initiated between ca. 18 and 10 Ma throughout the RGR, many faults record faster exhumation rates (~0.5 mm/yr to ~1.3 mm/yr; Figs. 3, 4, and 5). We find that faulting initiated fairly contemporaneously along the rift and that exhumation rates increased as new segments initiated and most-likely linked together (Abbey and Niemi, 2018). Understanding these faulting stages helps to differentiate between rift models and reveals that a northward propagating model is not well supported by evidence for the initiation of faulting from thermochronometric data along the RGR. To further discriminate between rift models, we next compare the spatial and temporal relationships between the rift-related faulting and rift-related magmatism.

5. RIO GRANDE RIFT MAGMATISM

Volcanic activity within rifts is commonly localized along major boundary faults, transfer zones, and limited portions of rift shoulders (i.e. off-axis volcanism) (Corti, 2012). Magmatism often assists with rifting and helps to transfer strain through ACZs (e.g. Rowland et al., 2007; 2010; Busby, 2013) by dike injection (Rowland et al., 2010; Stahl and Niemi, 2017). Volcanism in continental rift zones, grabens, and other manifestations of extensional tectonism is commonly dominated by mafic alkaline compositions (indicating an asthenospheric source) or has a bi-modal composition, in which case low-silica basalts and high silica rhyolites are erupted in the same location (e.g. Bailey, 1974; Tweto, 1979; Johnson and Thompson, 1991; Kellogg, 1999; Cosca et al., 2014).

5.1 Existing interpretations of Colorado and New Mexico volcanism

Cenozoic volcanism in Colorado and New Mexico is extensive and fairly continuous, and volcanism may not necessarily be an indicator of rift activity (Corti et al., 2019), thus using the history of volcanism to deduce the onset of rifting is challenging. Rather than using the timing of volcanism as a proxy for the onset of rifting, we find it is necessary to try and define or extract a particular signal from the nearly continuous Cenozoic volcanism to identify ‘rift-related’ magmatism. Previous studies suggest that rift-related magmatism in the RGR began between 29 and 26 Ma, when the style and chemical signature of volcanism changed from intermediate andesitic ignimbrites to eruptions of alkaline basalt and bi-modal lava compositions in Colorado and New Mexico (Epis and Chapin 1974; Lipman and Mehnert, 1975; Tweto, 1979; Lindsey et al., 1983; Miggins et al., 2002; Chapin et al., 2004). This transition is proposed to be associated with slab-rollback, retreat or detachment of the Farallon slab and subsequent development of the RGR (Cosca et al., 2014; Ricketts et al., 2015). However, most of the Cenozoic volcanic rocks in Colorado and New Mexico erupted outside the boundaries of the present-day rift. We therefore re-assess spatiotemporal patterns in volcanic ages and chemical compositions to determine what role magmatism has played in accommodating extension within the RGR.

5.2 Compilation of the Rio Grande rift volcanic data

We revisit the spatial, compositional and temporal evolution of magmatism in the greater RGR region using databases of volcanic rock information (EarthChem; http://www.earthchem.org/portal; accessed February 2018). We compiled chemical and age data related to all volcanic rocks in NM and CO with ages from 70 to 0 Ma (Table 4; more details on data compilation and filtering in supplementary data file).

To evaluate the hypothesis that rift-related volcanism began with a bi-modal alkaline signal at ~29-26 Ma we filter the information from EarthChem (Table 4; more details on data compilation and filtering in supplementary data file) and map the spatial extent of volcanism at several key time periods (Fig. 6). We also plot the frequency of lava composition as a function of time using major oxide composition data to discriminate between pre-rift and syn-rift volcanic rocks (Figs. 7 and S3). Major oxide data are more prevalent across the RGR than trace element or isotopic data, and thus we use the oxide compositional signature as a way to assess alkalinity of erupted volcanic rocks. Plotting these data on a Harker diagram of SiO_2 vs. Na_2O and K_2O, we find that there is no obvious temporal trend in the alkalinity signature of the Cenozoic volcanic rocks in CO and NM (Fig. S3). However, there is temporal variation in the wt% of SiO_2 seen in the volcanic rocks. We therefore assess the use of SiO_2 as a simple discriminant for a transition in eruption composition. We focus on lava 'compositions' as defined by the wt% of SiO_2 (e.g. <45% SiO_2, 45-52%, 53-63%, 63-70% and >70%; Figs. 6, 7, and S3).

5.3 Spatial and compositional evolution of volcanism in the RGR region

The oldest volcanism in our compilation spans from 70 to 40 Ma and is characterized by volcanic rocks of almost entirely intermediate to felsic compositions (>53% SiO_2; Fig. 7). Magmatism at that time was associated with the Laramide Orogeny and most of what is preserved is plutons, stocks, and plugs, with limited preservation of volcanic rock. The spatial extent of these rocks is limited to the Colorado Mineral Belt lineament in central CO, a southern belt in NM (Ortiz Mountains and Mogollon-Datil volcanic fields), and in west Texas along the TX and Mexico border (Fig. 6). From 40 Ma to 27 Ma, volcanic rocks are dominated by intermediate and felsic ignimbrites (>53% SiO_2; Fig. 7) that form several large volcanic fields (VF) outside the bounds (mostly west) of the present-day rift in both CO and NM (Thirty-nine Mile VF, San Juan VF and Mogollon-Datil VF; Figs. 6 and 7; e.g. Chapin et al., 2004). Between ~27 Ma and ~21

Ma, volcanism occurs almost exclusively via intermediate and rhyolitic eruptions in the Mogollon-Datil VF in southwestern New Mexico (Fig. 6; Chapin et al., 2004). In summary, late Eocene to Oligocene volcanism is intermediate to felsic in composition, is located, for the most part, west of the present-day RGR, and is attributed to slab foundering and rollback followed by mantle upwelling (McMillan et al., 2000; Chapin et al., 2004; Ricketts et al., 2015).

Throughout the early Miocene (~21-15 Ma), there is a lull in volcanism with only a few small-volume felsic to intermediate eruptions scattered around the Mogollon-Datil VF, San Juan VF, and Latir VF (Fig. 6). Renewed volcanism initiates in the middle Miocene (~15 Ma), and for the first time is spatially associated with the present-day extent of the RGR. During this phase of volcanism, mafic (<52% SiO_2) compositions become more prevalent (subequal quantities of mafic, intermediate and felsic lavas; Fig. 7; Chapin et al., 2004). Magmatism is focused in the central RGR in the Jemez, Taos, and Latir volcanic fields as well as some minor eruptions in the southern Albuquerque Basin (Fig. 6 and 8). By ca. 10 Ma, the prevalence of mafic volcanism increases, and eruptions occur primarily along the Jemez lineament in the Raton, Taos and Jemez VFs until ~2 Ma (Fig. 6). Minor late Miocene eruptions also occur in northwest CO in the Yampa VF at this time (Fig. 6; Cosca et al., 2014). From 2 Ma to present, volcanic eruptions are primarily mafic in composition and erupt along the Jemez Lineament in the McCarty’s, Mount Taylor, Ocate, and Raton-Clayton volcanic fields (Figs. 6 and 7). The Jemez VF is also active at this time, with eruptions of both basalt and rhyolite (i.e. Bandelier tuff; Chapin et al., 2004). Volcanic activity begins in the southern RGR after 2 Ma, with the eruption of low silica (<45 wt%) volcanic rock in the Jornada del Muerto, Carrizozo, and Potrillo VFs (Figs. 6 and 7).

The spatiotemporal patterns of dominantly intermediate to felsic compositions peripheral to the present-day RGR boundary and erupted prior to 21 Ma are markedly unlike the pattern of mafic eruptions that have occurred since ~15 Ma and which are located along the northeast-southwest trending Jemez lineament, crossing the central RGR (Fig. 6). Through this re-analysis we are unable to identify compelling evidence that supports previous suggestions that rift initiation can be documented by mafic and bi-modal magmatism during the Oligocene (Epis and Chapin 1974; Lipman and Mehnert, 1975; Tweto, 1979; Lindsey et al., 1983; Miggins et al., 2002; Chapin et al., 2004). Instead, voluminous mafic and bi-modal eruptions within the RGR begin in the middle Miocene, roughly 10 million years after fault initiation as determined by our thermochronometry analysis.

6. DISCUSSION

Our analysis of low-temperature thermochronometry data, interpretation of modeled fault-block thermal histories, and evaluation of spatiotemporal patterns of Cenozoic magmatism provides the means to assess rift development and mechanisms of extensional accommodation using a consistent approach throughout the entire extent of the Rio Grande rift. We use these data to (1) document the rift-wide onset of faulting as well as the processes of fault segment growth and linkage throughout the RGR. With this information we are able to (2) evaluate rift propagation models and further our analysis by combining faulting information with our re-analysis of regional magmatism to resolve spatial patterns in the mechanisms of extensional accommodation along the RGR. Hence, we are poised to ask the question of (3) whether along-rift changes in physiography are the product of evolutionary-stages, extension accommodation mechanisms, weakness from previous deformation events, characteristics of the crust and lithosphere beneath the surface of the rift, or some combination of these factors.

6.1 Initiation, Growth, and Integration of the Rio Grande Rift system

Here we use our complied and modelled thermochronometry data in combination with our summary of regional Cenozoic magmatism to address the development, growth, and integration of the RGR.

6.1.1 Thermochronometric constraints on spatial and temporal patterns of rift-related fault initiation and growth

To understand fault growth and rift basin connection in the RGR we have taken an approach similar to that presented by Abbey and Niemi (2018) who showed that a multi-transect approach is a viable method for identifying rift initiation and quantifying fault growth patterns. Their work focused on vertical transects from the upper Arkansas River (UAR) Basin, which documented phases of segment initiation occurring at ~25 Ma, and ~18 Ma, and fault exhumation acceleration which was inferred to be related to fault growth via tip propagation and segment linkage (Kim and Sanderson, 2005, Curry et al., 2016), a process which appears to occur over a span of several millions of years (Abbey and Niemi, 2018).

Fault initiation along the length of the entire RGR occurred at ~25 Ma in a number of transects, similar to the onset of exhumation observed from the densely sampled UAR Basin (Abbey and Niemi, 2018). Other transects throughout the RGR record a later onset of exhumation, which we infer to reflect individual fault segment initiation and growth (Fig. 9). Rift-wide, we observe an increase in the rate of exhumation in the middle to late Miocene, similar to the timing of exhumation rate increase observed in the UAR Basin (Abbey and Niemi, 2018), and the subsidence records from the central rift basins (van Wijk et al., 2018). Interpretation of the inverse thermal history models of the thermochronometric data suggests that each of the rift basins, with the exception of the Española Basin in the central RGR, developed through a process of fault segment initiation followed by tip growth and linkage over the course of 10 to 15 million years, similar to the pattern observed in the UAR basin where the density of thermochronometric data is greatest (Figs. 8 and 9). Thus, by ~15 to 10 Ma fault segments within each individual rift basin became linked, forming the main basin-bounding faults we observe today. Once linked, the rift-bounding faults continued to grow and by ~10-5 Ma individual basins began to connect via accommodation zones (Figs. 3, 4, 5, and 9).

Accommodation zones aid in strain transfer and basin integration in different ways throughout the RGR. For example, the Poncha Pass ACZ transfers strain between the San Luis Basin and the UAR Basin along a narrow region of northeast-southwest striking faults which developed in the late Miocene (Hubbard et al., 2001; Kellogg et al., 2017; Minor et al., 2019). In the central and southern RGR, strain transfer is more commonly accommodated via magmatic injection (e.g. Casey et al., 2006; Keir et al., 2006), and across broad areas of overlapping faults that gradually transfer displacement (e.g. Lewis and Baldridge, 1994; Fig. 9). For example, the Tijeras, Santa Ana, and Embudo ACZs in the central RGR are associated with voluminous volcanism, numerous strike-slip faults, and a concentration of intra-basin faults that began accommodating oblique slip and strain transfer in the middle Miocene (e.g. Fig. 9; Grauch et al., 2017). In contrast to the central RGR ACZs, which contain notable surface faults and eruptive volcanism, the Cutter Sag transfer zone and Socorro ACZ in the southern RGR exist in a region with little to no fault expression or volcanism at the surface but evidence for large subsurface magmatism (e.g. Fig. 9; Sanford et al., 1977; Mack and Seager, 1995; Balch et al., 1997).

The fault initiation, growth, and linkage patterns we observe from our new thermal history modeling reveals a framework in which individual fault segments link to become large-basin-bounding faults. Each basin-bounding fault then continues to develop by transferring strain across accommodation zones, frequently with the help of magmatic injection.

6.1.2 Strain transfer and basin connection through magmatically driven accommodation zones

Magmatism within the RGR is almost exclusively found in the central part of the rift. Eruptive magmatism, however, is not present in the central RGR until the middle Miocene, and the lack of regional magmatism suggests that the onset of magmatism cannot be used as an indicator for whole rift initiation, although it is a potentially useful indicator for understanding spatial variability in the mechanisms of extensional accommodation. The lack of thermochronometric ages <30 Ma in the central RGR suggest minimal displacement on surface-breaking normal faults in the central RGR (Fig. 4; Kelley, 1990), and the evidence that seismicity in this region is associated with the major magmatic centers rather than the large strike-slip faults (Nakai et al., 2017) indicates that the connection between the northern and southern RGR is accommodated predominantly by magma injection processes rather than tectonic processes (Figs. 4, 9 and 10; Kelson et al., 2004; Grauch et al., 2017). Therefore, the central part of the rift appears to be the sole region where rifting is primarily accommodated by magmatism. The timing of eruptive magmatism in the central RGR coincides with an increase in exhumation rates rift-wide and may reflect the development of magmatic-dominated ACZs connecting basins from the northern RGR (San Luis Basin) to the southern RGR (Albuquerque Basin).

Volcanism within the bounds of the rift also occurs in the southern RGR, where basaltic eruptions have occurred post-2 Ma (Figs. 6, 8 and 9). Minor, low-silica basaltic eruptions are common in extensional settings such as Death Valley (e.g. Manley et al., 2000) and Lunar Crater (e.g. Scott and Trask, 1971; Valentine and Cortés, 2013) in the Basin and Range, and in the southern RGR this magmatism appears to play a role in transferring strain through dike injection into established ACZs in the southern RGR (Fig. 9; Mack and Seager, 1995). We hypothesize that the majority of the extension in the southern RGR is accommodated via faulting on the large interconnected north-south striking basin-bounding normal faults where thermochronometric cooling ages range from ~20 to 5 Ma (Fig. 3; Kelley and Chapin, 1997) and that integration between the Albuquerque Basin and southernmost RGR basins occurs through magmatism within the southern accommodation and transfer zones, as evidenced by the active eruptive centers, subsurface magma bodies, and seismicity related to dike injection (e.g. Sanford et al., 1977; Balch et al., 1997; Nakai et al., 2017) (Fig. 9). Therefore, we suggest that although rift initiation was mainly tectonically driven, integration of the whole rift system was magma assisted.

6.1.3 Summary of RGR growth and integration of rift basins

The integration and accommodation of the entire RGR occurs through a combination of both faulting and magmatism. As faults and basins grew and linked in the northern and southern RGR through the middle Miocene, rifting was accommodated through magmatic injection in the central RGR (Figs. 6, 7, 8, and 9). Linking between individual basins began in the middle Miocene, connecting the San Luis Basin, Española Basin and Albuquerque Basin through active magmatism (Figs. 8 and 9). In the northern and southern RGR basins linkage occurs in the late Miocene, with linkage in the north occurring from continued growth of basin-bounding faults, and linkage in the south from a combination of fault growth and minor Quaternary volcanism (Figs. 8 and 9). We can document this in the slowly evolving RGR and find that fault segment linkage within a single basin can take 10-15 m.y. after fault initiation and that integration between basins can take another 5-10 m.y. to fully develop. Thus, even though several parts of the rift initiated synchronously, and sections of the rift have been actively accommodating extension since ca. 25 Ma, the development of a fully integrated system of connected rift basins did not occur until ~ 5 Ma (Figs. 8 and 9).

6.2 Controls on Rift Physiography from Inherited Structures and Lithospheric Architecture

Observed differences in physiography and accommodation style in continental rifts globally are not reflective of a continuum of rift evolutionary stages, but rather must be related to other factors that influence extensional processes, such as inherited crustal weaknesses and/or lithospheric architecture (Buck, 1991; Brun, 1999; Corti, 2012; Fletcher et al. 2018; Corti et al., 2018). Significant differences in lithospheric thickness exist throughout much of the western U.S., and around the Colorado Plateau (e.g. Levander et al., 2011). Within the RGR, the depth to the lithosphere-asthenosphere boundary (LAB) shallows from >100 km beneath the Colorado Plateau and northern RGR to 60-70 km beneath the Basin and Range and southern RGR (Levander et al., 2011; Fig. 10).

Consequently, the northern RGR faults are rupturing a region where lithospheric thicknesses are >100 km (Levander et al., 2011), and the southern RGR faults are rupturing an ~65 km thick lithosphere (Fig. 10; Levander et al., 2011). These differences in thickness may account for differences in the styles of faulting seen in the northern and southern RGR, as wider, more diffuse rift zones are often associated with thinner and warmer underlying lithosphere as opposed to narrow, deep grabens that are found in areas with a cold, thick lithosphere (Buck, 1991; Ebinger, 1991; Ebinger, 2005). The step in the LAB in the central RGR also occurs along the Jemez lineament, and is spatially coincident with known Proterozoic terrane boundaries (e.g. the suture between the Yavapai and Mazatzal terranes; Fig. 10; Karlstrom and Bowring, 1988; Karlstrom and Humphreys, 1998; Shaw and Karlstrom, 1999; Chapin et al., 2004; Chapin, 2012). The formation of the active volcanic centers of the Jemez lineament over this LAB step suggests that inherited structure from ancient features continues to play a role in controlling deformation in the region (Baldridge et al., 2006). Similar to the RGR, changes in rift deformation style occur in the East African rift system and are coincident with 'steps' in crustal thickness attributed to deep-seated Neoproterozoic sutures and other inherited weaknesses (e.g. Boone et al., 2019; Corti et al., 2019), suggesting that such controls are common in continental rift systems.

Abrupt lithospheric thickness changes not only suggest inheritance from pre-existing weaknesses caused by previous deformation events, but also appear to have strong controls on the localization of magmatism (e.g. Corti et al., 2019). Beyond the recognized extent of the RGR, large volcanic eruptions occur along the entire length of the Jemez lineament, and around the Colorado Plateau at the transition between the plateau and the Basin and Range. An abrupt change in lithospheric thickness is most prominent along this transition (Fig. 10), and others have recognized such steps in lithospheric thickness can be a mechanism for driving magmatism, for example, through edge-driven convection (e.g. van Wijk et al., 2010; Levander et al., 2011; Rudzitis et al., 2016; Fig. 10).

Our estimated exhumation magnitudes and rates determined from thermal history modeling along with the localized patterns seen in Cenozoic magmatism further emphasizes the physiographic differences that exist between the southern, central, and northern RGR. Although a detailed exploration of crustal inheritance and regional pre-existing structure is beyond the scope of this work, we propose that crustal and lithospheric properties (i.e. thickness and potentially age and rheology) control rift accommodation and play a role in the orientation of faulting and magmatism along the RGR, as seen in continental rifts elsewhere (Fig. 10; e.g. Brun, 1999; Corti, 2012; Fletcher et al. 2018; Corti et al., 2018; Corti et al., 2019). Therefore, we suggest that differences in rift accommodation mechanisms (i.e. faulting vs. magmatism), are likely controlled by deep-seated lithospheric-scale properties and architecture, rather than progressive stages of rift development (e.g. Corti, 2012).

We hypothesize that pre-existing structures from ancient terranes, such as the suture between the Yavapai and Mazatzal terranes, influence faulting style within the RGR (i.e. single-basin-bounding faults at a given latitude, strike-slip faults and intra-basin faults, and several basin-bounding faults at a given latitude), and encourages the localization of magmatic accommodation (i.e. through edge-driven convection along the Jemez lineament). Hence, RGR accommodation mechanisms and styles of deformation seem to be highly spatially controlled by pre-existing weaknesses *and* lithospheric structure as opposed to a temporal evolution of deformation from south to north.

6.3 Rio Grande Rift model

Our analysis of thermochronometry and magmatism within the RGR rules out rift models involving time progressive propagation of rifting (northward propagation in the case of the RGR). Accordingly, we consider generalized synchronous rifting models—block rotation and oblique strain, as possible mechanisms driving the development of the RGR (Fig. 1; e.g. Ebinger, 1984; Nelson et al., 1992; Brune et al., 2017; Molnar et al., 2017; Brune et al., 2018).

The greater magnitudes of horizontal extension in the southern RGR as compared to the northern RGR and the thermochronometric evidence for synchronous faulting in both regions is consistent with a block rotation model. In fact, paleomagnetic and geodetic studies argue for clockwise rotation of the Colorado Plateau, also supporting a block rotation model for RGR opening (Zoback and Thompson, 1978; Kelley, 1979; Hamilton, 1981; Cordell, 1982; Golombek et al., 1983; Brown and Golombek 1986; Lewis and Baldridge, 1994; Chapin and Cather, 1994; Kreemer et al., 2010; McCall and Kodama, 2014). However, this rotation is suggested to have occurred in the middle to late

Miocene (i.e. 10-15 million years after rift initiation as determined by our thermochronometric data analysis). Therefore, we cannot rule out an oblique strain model especially in light of a recent global rifting study which showed that the majority of rifting is accomplished from oblique strain (Brune et al., 2018). We suggest that rifting is driven by a combination of oblique strain and block rotation, mechanisms which evolve with the changing far-field plate boundary conditions through time. Our hybrid rift model entails that rifting began in a style similar to an oblique strain model (Fig. 1), with initiation in both the northern and southern RGR, followed by a linkage across a weak zone (the Jemez Lineament) and then was enhanced by block rotation in the middle to late Miocene, accounting for the greater extension magnitudes in the southern RGR (Fig. 1).

7. CONCLUSIONS

Assessment of spatiotemporal relationships between rift-related faulting and magmatism in the RGR suggests synchronous rift initiation at ca. 25 Ma on several separate fault segments. Fault-segment-initiation, growth, and linkage continued for 10 to 15 m.y. and magmatic accommodation in the central RGR helped to fully integrate the rift into one connected system by the late Miocene. Inherited crustal and lithospheric structure appear to play a role in controlling the surface expression and extension accommodation within continental rifts (e.g. thickness). We find that understanding rift accommodation via spatiotemporal patterns in faulting and magmatism is necessary to distinguish between competing rift initiation and growth models and may be useful for discriminating between models of continental rifting processes. Per our new understanding of controls on continental rifting processes and accommodation mechanisms, we propose that components of both oblique strain and block rotation (i.e. clockwise rotation of the Colorado Plateau) drove rifting in the RGR. Here we emphasize that understanding continental rift initiation and development through assessment of the spatiotemporal relationships between both faulting and magmatism is useful for distinguishing between rifting processes and accommodation controls and can help to determine processes and factors controlling the evolution of continental rift systems around the world.

ACKNOWLEDGEMENTS

We thank K.E. Murray for assistance with sample collection and for insightful conversations about western U.S. geology. We thank Amanda Maslyn (University of Michigan) and Victor Valencia (ZirChron LLC) for assistance with sample processing and analysis. We thank S. Baldridge and an anonymous reviewer for insightful questions and comments on previous versions of this manuscript. This work was partially supported by NSF grant EAR-1151247 (NAN), as well as a Rackham graduate student research grant and a Turner Award from the Department of Earth and Environmental Sciences at the University of Michigan (ALA). All new analytical data collected as part of this study are included in the manuscript and in supplementary files; in addition the data can be found in the UM Deep Blue repository at https://doi.org/10.7302/cvn3-eq83.

REFERENCES

Abbey, A. L., & Niemi, N. A. (2018). Low-temperature thermochronometric constraints on fault initiation and growth in the northern Rio Grande rift, upper Arkansas River valley, Colorado, USA. *Geology, 46*(7), 627-630. doi:10.1130/G40232.1

Abbey, A. L., Niemi, N. A., Geissman, J. W., Winkelstern, I. Z., & Heizler, M. (2017). Early Cenozoic exhumation and paleotopography in the Arkansas River valley, southern Rocky Mountains, Colorado. *Lithosphere*, *10*(2), 239-266. doi:10.1130/L673.1

Bailey, D. K. (1974). Continental rifting and alkaline magmatism. In Sorensen, H. (Ed.), *The alkaline rocks*. New York, Wiley, 148–159.

Balch, R. S., Hartse, H. E., Sanford, A. R., & Lin, K. (1997). A new map of the geographical extent of the Socorro mid-crustal magma body. *Bulletin of Seismological Society of America*, *87*, 174-182.

Baldridge, W. S., Keller, G. R., Haak, V., Wendlandt, E., Jiracek, G. R., & Olsen, K. H. (2006). The Rio Grande rift. In *Developments in Geotectonics* (Vol. 25, pp. 233-XIII). Elsevier.

Baldridge, W. S., Ferguson, J. F., Braile, L. W., Wang, B., Eckhardt, K., Evans, D., ... & Biehler, S. (1994). The western margin of the Rio Grande Rift in northern New Mexico: An aborted boundary?. *Geological Society of America Bulletin*, *106*(12), 1538-1551.

Biehler, S., Ferguson, J., Baldridge, W. S., Jiracek, G. R., Aldern, J. L., Martinez, M., ... & Hersey, D. R. (1991). A geophysical model of the Española basin, Rio Grande rift, New Mexico. *Geophysics*, *56*(3), 340-353.

Boone, S. C., Balestrieri, M. L., Kohn, B. P., Corti, G., Gleadow, A. J. W., & Seiler, C. (2019). Tectono-thermal evolution of the Broadly Rifted Zone, Ethiopian Rift. *Tectonics*.

Brister, B. S. & Gries, R. R. (1994). Tertiary stratigraphy and tectonic development of the Alamosa basin (northern San Luis basin), Rio Grande rift, south-central Colorado. In Keller, G. R. & Cather, S. M. (Eds.), *Basins of the Rio Grande rift: Structure, stratigraphy, and tectonic setting. Geological Society of America Special Paper*, *291*, 39–58.

Brown, L. L., & Golombek, M. P. (1986). Block rotations in the Rio Grande rift, New Mexico. *Tectonics, 5*, 423-438.

Brun, J. P. (1999). Narrow rifts versus wide rifts: inferences for the mechanics of rifting from laboratory experiments. *Philosophical Transactions of the Royale Society 138 London Series A-Mathematical, Physical and Engineering Sciences, 357*, 695-710.

Brune, S., Corti, G., & Ranalli, G. (2017). Controls of inherited lithospheric heterogeneity on rift linkage: Numerical and analogue models of interaction between the Kenyan and Ethiopian rifts across the turkana depression. *Tectonics, 36,* 1767-1786.

Brune, S., Williams, S. E., & Müller, R. D. (2018). Oblique rifting: the rule, not the exception. *Solid Earth*, *9*(5).

Bryant, B., & Naeser, C. W. (1980). The significance of fission-track ages of apatite in relation to the tectonic history of the Front and Sawatch Ranges, Colorado. *Geological Society of America Bulletin*, *91*, 156–164.

Buck, W. R. (1991). Modes of continental lithospheric extension. *Journal of Geophysical Research: Solid Earth*, *96*(B12), 20161–20178.

Buck, W. R. (2004). Consequences of asthenospheric variability on continental rifting, In Karner, G. D., Taylor, B., Droscoll, N. W., & Kohlstedt, D. L. (Eds.), *Rheology and Deformation of the Lithosphere at Continental Margins*. Columbia University Press, New York, 1-30.

Buck, W. R. (2006). The role of magma in the development of the Afro-Arabian Rift System. *Geological Society, London, Special Publications*, *259*(1), 43-54.

Busby, C. J. (2013). Birth of a plate boundary at ca. 12 Ma in the Ancestral Cascades arc, Walker Lane belt of California and Nevada. *Geosphere, 9*(5), 1147–1160.

Casey, M., Ebinger, C., Keir, D., Gloaguen, R., & Mohamed, F. (2006). Strain accommodation in transitional rifts: extension by magma intrusion and faulting in Ethiopian rift magmatic segments. *Geological Society, London, Special Publications*, *259*(1), 143-163.

Chai, C., Ammon, C. J., Maceira, M., & Herrmann, R. B. (2015). Inverting interpolated receiver functions with surface wave dispersion and gravity: Application to the western US and adjacent Canada and Mexico. *Geophysical Research Letters*, *42*(11), 4359-4366.

Chapin, C. E. (2012). Origin of the Colorado mineral belt. *Geosphere, 8*(1), 28-43.

Chapin, D. E., & Cather, S. M. (1994). Tectonic setting of the axial Basins of northern and central Rio Grande Rift. In Keller, G. R., and Cather, S. M. (Eds.), *Basins of the Rio Grande Rift: structure stratigraphy and tectonic setting: Geological Society of America Special Publication* (Vol. 291, pp. 5-25).

Chapin, C. E., & Seager, W. R, (1975). Evolution of the Rio Grande rift in the Socorro and Las Cruces areas. *26th Field Conference, New Mexico Geological Society*, 297-321.

Chapin, C. E., Wilks, M., & McIntosh, W. C. (2004). Space-time patterns of late Cretaceous to present magmatism in New Mexico-comparison with Andean volcanism and potential for future volcanism. In Cather, S. M., McIntosh, W. C., & Kelley, S. A. (Eds.). *Tectonics, geochronology, and volcanism in the southern Rocky Mountains and Rio Grande rift* (Vol. 160, pp. 13–40). Socorro, New Mexico: Bureau of Geology and Mineral Resources Bulletin.

Contreras, J., Anders, M. H., & Scholz, C. H. (2000). Growth of a normal fault system: observations from the Lake Malawi basin of the east African rift. *Journal of Structural Geology*, *22*(2), 159-168.

Cordell, L. (1982). Extension in the Rio Grande rift. *Journal of Geophysical Research, 87*, 8561–8569.

Corti, G. (2008). Control of rift obliquity on the evolution and segmentation of the main Ethiopian rift. *Nature Geoscience*, *1*(4), 258.

Corti, G. (2009). Continental rift evolution: from rift initiation to incipient break-up in the Main Ethiopian Rift, East Africa. *Earth Science Reviews, 96*, 1-53.

Corti, G., (2012). Evolution and characteristics of continental rifting: analogue modeling-inspired view and comparison with examples from the East African Rift System. *Tectonophysics, 522-523,* 1-33.

Corti, G., Molin, P., Sembroni, A., Bastow, I. D., & Keir, D. (2018). Control of pre-rift lithospheric structure on the architecture and evolution of continental rifts: Insights from the Main Ethiopian Rift, East Africa. *Tectonics*, *37*(2), 477-496.

Corti, G., Cioni, R., Franceschini, Z., Sani, F., Scaillet, S., Molin, P., ... & Erbello, A. (2019). Aborted propagation of the Ethiopian rift caused by linkage with the Kenyan rift. *Nature communications*, *10*(1), 1309.

Cosca, M. A., Thompson, R. A., Lee, J. P., Turner, K. J., Neymarl, L. A., & Premo, W. R., (2014). ^{40}Ar/^{39}Ar geochronology, Isotope geochemistry (Sr, Nd, Pb), and petrology of alkaline lavas near Yampa, Colorado: Migration of alkaline volcanism and evolution of the northern Rio Grande rift. *Geosphere, 10*(2), 374-400.

Cunningham, C. G., Naeser, C. W., & Marvin, R. F. (1977). New ages for intrusive rocks in the Colorado mineral belt. *U.S. Geological Survey Open-File Report 77-573,* 7p.

Curry, M. A., Barnes, J. B., and Colgan, J. P., (2016). Testing fault growth models with low-temperature thermochronology in the northwest Basin and Range, USA. *Tectonics*, *35*, 2467–2492. doi:10.1002/2016TC004211.

Dean, R. B., & Dixon, W. J. (1951). Simplified Statistics for Small Numbers of Observations. *Analytical Chemistry, 23*(4), 636–638.

Duller, R. A., Whittaker, A. C., Swinehart, J. B., Armitage, J. J., Sinclair, H. D., Bair, A., Allen, P. A. (2012). Abrupt landscape change post–6 Ma on the central Great Plains, USA. *Geology, 40*(10), 871–874.

Ebinger, C. J. (1989). Tectonic development of the western branch of the East African rift System. *GSA Bulletin, 101*(7), 885–903.

Ebinger, C. (2005). Continental break-up: the East African perspective. *Astronomy & Geophysics*, *46*(2), 2-16.

Ebinger, C., Crow, M., Rosendahl, B., Livingstone, D., & Le Fournier, J. (1984). Structural evolution of Lake Malaŵi. *Nature*, *308*, 627-629.

Ebinger, C. J., Karner, G. D., & Weissel, G. D. (1991). Mechanical strength of extended continental lithosphere: constraints from the western rift system, Africa. *Tectonics*, *10*, 1239-1256.

Ebinger, C. J., van Wijk, J., & Keir, D. (2013). The time scales of continental rifting: Implications for global processes. In Bickford, M. E. (Ed.), *The Web of Geological Sciences: Advances, Impacts, and Interactions: Geological Society of America Special Paper 500*, 371–396.

Ehlers, T. A. (2005). Crustal Thermal Processes and the Interpretation of Thermochronometer Data. *Reviews in Mineralogy and Geochemistry, 58*(1), 315–350.

Epis, R. C., & Chapin, C. E. (1974). Stratigraphic Nomenclature of the Thirty-nine Mile Volcanic Field, Central Colorado. *Geologic Survey Bulletin*, 1–32.

Epis, R. C., Scott, G. R., Taylor, R. B., & Chapin, C. E. (1976). Cenozoic Volcanic, Tectonic, and Geomorphic Features of Central Colorado. *Studies in Colorado Field Geology, Professional Contributions Colorado School of Mines*, 323–338.

Farley, K. A. (2002). (U-Th)/He Dating: Techniques, Calibrations, and Applications. *Reviews in Mineralogy and Geochemistry, 47*(1), 819–844.

Fletcher, A. W., Abdelsalam, M. G., Emishaw, L., Atekwana, E. A., Laó-Dávila, D. A., & Ismail, A. (2018). Lithospheric controls on the rifting of the Tanzanian craton at the Eyasi basin, eastern branch of the East African rift system. *Tectonics, 37*, 2818–2832.

Flowers, R. M., Ketcham, R. A., Shuster, D. L., & Farley, K. A. (2009). Apatite (U–Th)/He thermochronometry using a radiation damage accumulation and annealing model. *Geochimica et Cosmochimica Acta, 73*(8), 2347–2365.

Frankel, K. L., & Pazzaglia, F. J. (2006). Mountain fronts, base-level fall, and landscape evolution: Insights from the southern Rocky Mountains. In Special Paper 398: *Tectonics, Climate, and Landscape Evolution* (Vol. 398, pp. 419–434), Geological Society of America.

Gallagher, K., Stephenson, J., Brown, R., Holmes, C., Fitzgerald, P. (2005). Low temperature thermochronology and modeling strategies for multiple samples 1: vertical profiles. *Earth and Planetary Science Letters 237*, 193–208. https://doi.org/10.1016/J.EPSL.2005.06.025.

Gallagher, K. (2012). Transdimensional inverse thermal history modeling for quantitative thermochronology. *Journal of Geophysical Research, 117*(B2).

Golombek M. D., McGill G. E., & Brown L. (1983). Tectonic and geologic evolution of the Espanola Basin, Rio Grande Rift: structure, rate of extension and relation to the state of stress in the Western United States. *Tectonophysics, 94*, 483-507.

Grauch, V. J. S., Bauer, P. W., Drenth, B. J., Kelson, K. I. (2017). A shifting rift—Geophysical insights into the evolution of Rio Grande rift margins and the Embudo transfer zone near Taos, New Mexico. *Geosphere, 13*(3), 870–910.

Guenthner, W. R., Reiners, P. W., Ketcham, R. A., Nasdala, L., & Giester, G. (2013). Helium diffusion in natural zircon: Radiation damage, anisotropy, and the interpretation of zircon (U-Th)/He thermochronology. *American Journal of Science*, *313*(3), 145-198.

Hamilton, W. (1981). Plate-tectonic mechanism of Laramide deformation. *Contributions in Geology*, *1*9, 87-92.

Heller, P. L., Dueker, K., & McMillan, M. E. (2003). Post-Paleozoic alluvial gravel transport as evidence of continental tilting in the US Cordillera. *Geological Society of America Bulletin*, *115*(9), 1122-1132.

House, M. A., Kelley, S. A., & Roy, M. (2003). Refining the footwall cooling history of a rift flank uplift, Rio Grande rift, New Mexico. *Tectonics*, *22*(5), 1060.

Hubbard, M. S., Oviatt, C. G., Kelley, S., Perkins, M. E., Hodges, K. V., & Robbins, R. (2001). Oligocene-Miocene basin formation and modification in the northern Rio Grande rift; constraints from $^{40}Ar/^{39}Ar$, fission track, and tephrochronology. *Geological Society of America Abstracts with Programs*, *33*(6), A-257.

Ingersoll, R. V. (2001). Structural and stratigraphic evolution of the Rio Grande Rift, northern New Mexico and southern Colorado. *International Geology Review*, *43*(10), 867-891.

Johnson, C. M., & Thompson, R. A. (1991). Isotopic composition of Oligocene mafic volcanic rocks in the northern Rio Grande rift: Evidence of contributions of ancient intraplate and subduction magmatism to evolution of the lithosphere.*Journal of Geophysical Research*, *96*, 13,593-13,608.

Johnstone, S. A., & Colgan, J. P. (2018). Interpretation of low-temperature thermochronometer ages from tilted normal fault blocks. *Tectonics*, *37*(10), 3647-3667.

Karlstrom, K. E., Harlan, S., Williams, M., McClelland, J., Geissman, J. W., & Ahäll, K. I. (1999). Refining Rodinia: Geologic evidence for the Australia–Western U.S. (AUSWUS) connection for Proterozoic supercontinent Reconstructions. *GSA Today*, *9*, 1–7.

Karlstrom, K. E., & Bowring, S. A. (1988). Early Proterozoic Assembly of Tectonostratigraphic Terranes in Southwestern North America. *The Journal of Geology*, *96*(5), 561-576.

Karlstrom, K. E., & Humphreys, E. D. (1998). Persistent influence of Proterozoic accretionary boundaries in the tectonic evolution of southwestern North America, Interaction of cratonic grain and mantle modification events. *Rocky Mountain Geology*, *33*(2), 161–179.

Keir, D., Ebinger, C. J., Stuart, G. W., Daly, E., & Ayele., A. (2006). Strain accommodation by magmatism and faulting as rifting proceeds to breakup: Seismicity of the northern Ethiopian rift. *Journal of Geophysical Research: Solid Earth*, *111*(B5).

Kelley, S. (1990). Late Mesozoic to Cenozoic cooling histories of the Sangre de Cristo Mountains, Colorado and New Mexico. In Bauer, P. W., Lucas, S. G., Mawer, C. K., & McIntosh, W. C., (Eds.), *Tectonic Development of the Southern Sangre de Cristo Mountains, New Mexico: New Mexico Geological Society 41st Annual Fall Field Conference Guidebook*, p. 123-132.

Kelley, S. A., Chapin, C. E., & Corrigan, A. J. (1992). Late Mesozoic to Cenozoic Cooling Histories of the Flank of the Northern and Central Rio Grande Rift, Colorado and New Mexico. *New Mexico Bureau of Mines Mineral Resources, 145*, 1–40.

Kelley, S. A., & Chapin, C. E. (1995). Apatite Fission-Track Thermochronology of Southern Rocky Mountain-Rio Grande Rift-Western High Plains Provinces. *New Mexico Geological Society Guidebook, 46*, 87–96.

Kelley, S. A., & Chapin, C. E. (1997). Cooling histories of mountain ranges in the southern Rio Grande rift based on apatite fission-track analysis—a reconnaissance survey. *New Mexico Bureau of Mines Mineral Resources, 19*(1), 1–14.

Kelley, S. A., & Duncan, I. J. (1986). Late Cretaceous to Middle Tertiary tectonic history of the northern Rio Grande rift, New Mexico. *Journal of Geophysical Research, 91*, 6246-6262.

Kelley, V. C. (1979). Tectonics, middle Rio Grande rift, New Mexico. *Rio Grande rift: tectonics and magmatism*, *14*, 57-70.

Kellogg, K. S. (1999). Neogene basins of the northern Rio Grande rift: partitioning and asymmetry inherited from Laramide and older uplifts. *Tectonophysics, 305*, 141-152.

Kellogg, K. S., Shroba, R. R., Ruleman, C. A., Bohannon, R. G., McIntosh, W. C., Premo, W. R., ... & Brandt, T. R. (2017). *Geologic map of the upper Arkansas River valley region, north-central Colorado* (No. 3382). US Geological Survey.

Kelson, K. I., Bauer, P. W., Unruh, J. R., & Bott, D. J. (2004). Late Quaternary characteristics of the northern Embudo fault, Taos County, New Mexico. In

Brister, B. S., Bauer, P. W., Read, A. S., & Lueth, V. W. (Eds.), *New Mexico Geological Society Guidebook: 55th Field Conference, Geology of the Taos Region*, 147–157.

Kim, Y. S., & Sanderson, D. J. (2005). The relationship between displacement and length of faults: a review. *Earth-Science Reviews*, *68*(3-4), 317-334.

Kluth, C. F., Schaftenaar, C. H. (1994). Depth and geometry of the northern Rio Grande Rift in the San Luis Basin, south-central Colorado. In Keller, G. R., & Cather, S. M. (Eds.), *Basins of the Rio Grande Rift: Structure, stratigraphy and tectonic setting*. Geological Society of America Special Paper 291, 27–38.

Knepper, D. H. Jr. (1974). Tectonic analysis of the Rio Grande rift zone, central Colorado. [Doctoral Thesis] Colorado School of Mines, Golden, CO.

Koning, D. J., Aby, S., Grauch, V. J. S., & Zimmerer, M. J. (2016). Latest Miocene–earliest Pliocene evolution of the ancestral Rio Grande at the Española–San Luis Basin boundary, northern New Mexico. *New Mexico Geology*, *38*(2), 24-49.

Kreemer, C., Blewitt, G., & Bennett, R. A. (2010). Present-day motion and deformation of the Colorado Plateau. *Geophysical Research Letters*, *37*(10), 1-5.

Landman, R., & Flowers, R. M. (2013). (U-Th)/He thermochronologic constraints on the evolution of the northern Rio Grande Rift, Gore Range, Colorado, and implications for rift propagation models. *Geosphere*, *9*(1), 170–187.

Lavecchia, A., Thieulot, C., Beekman, F., Cloetingh, S., & Clark, S. (2017). Lithosphere erosion and continental breakup: Interaction of extension, plume upwelling and melting. *Earth and Planetary Science Letters, 467*, 89-98.

Leat P. T., Thompson, R. N., Dickin, A. P., Morrison, M. A., & Hendry, G. L. (1989). Quaternary volcanism in northwestern Colorado: Implications for the roles of asthenosphere and lithosphere in the genesis of continental basalts. *Journal of Volcanism Geothermal Research*, *37*, 291-310.

Leat P. T., Thompson, R. N., Morrison, M. A., Hendry, G. L., & Dickin A. P. (1990). Geochemistry of mafic lavas in the early Rio Grande rift, Yarmony Mountain, Colorado, U.S.A. *Chemical Geology*, *81*, 23-43.

Leonard, E. M. (2002). Geomorphic and tectonic forcing of late Cenozoic warping of the Colorado piedmont. *Geology*, *30*(7), 595–598.

Leonard, E. M., Hubbard, M. S., Kelley, S. A., Evanoff, E., Siddoway, C. S., Oviatt, C. G., Heizler, M., &Timmons, M. (2002). High Plains to Rio Grande rift: Late Cenozoic evolution of central Colorado. *In Geological Society of America Meeting Field Trip Guidebook: Geological Society of America, Boulder, Colorado*, 35 p.

Levander, A., Schmandt, B., Miller, M. S., Liu, K., Karlstrom, K. E., Crow, R. S., Lee, C. T .A., & Humphreys, E. D. (2011). Continuing Colorado plateau uplift by delamination style convective lithospheric down-welling. *Nature*, *472*, 461-466.

Lewis C. J., Baldridge W. S. (1994). Crustal extension in the Rio Grande rift, New Mexico: Half-grabens, accommodation zones, and shoulder uplifts in the Ladron Peak-Sierra Lucero area. *Geological Society of America, Special Paper*, *291*, 135-155.

Limbach, F. W. (1975). The geology of the Buena Vista area, Chaffee county, Colorado: [Doctoral Thesis]. Colorado School of Mines, Golden, Colorado, T-1692.

Lipman, P. W., & Mehnert, H. H. (1975). Late Cenozoic basaltic volcanism and development of the Rio Grande depression in the Southern Rocky Mountains. In Curtis, B. F. (Ed.), *Cenozoic history of the southern Rocky Mountains: Geological Society of America Memoir, 144*, 119–154.

Lindsey, D. A., Andriessen, P. A. M., & Wardlaw, B. R. (1986). Heating, cooling, and uplift during Tertiary time, northern Sangre de Cristo Range, Colorado. *Geological Society of America Bulletin, 97*, 1133-1143.

Lindsey, D. A., Lohnson, B. R., & Andriessen, P. A. M. (1983). Laramide and Neogene structure of the northern Sangre de Cristo Range, south-central Colorado. In Lowell, J. D. (Ed.), *Rocky Mountain Foreland Basins and Uplifts*. Rocky Mountain Association of Geology, Denver, CO, 219–228.

Liu, Y. A., Murphy, M. A., van Wijk, J., Koning, D. J., Smith, T., & Andrea, R. A. (2019). Progressive opening of the northern Rio Grande rift based on fault structure and kinematics of the Tusas-Abiquiu segment in north-central New Mexico, US. *Tectonophysics, 753*, 15-35.

Lozinsky, R. P. (1988). Stratigraphy, sedimentology, and sand petrology of the Santa Fe Group and pre-Santa Fe Tertiary deposits in the Albuquerque basin, central New Mexico. [Doctoral Thesis], New Mexico Institute of Mining and Technology, Socorro, New Mexico.

Machette, M. N. (1988). Quaternary movement along the La Jencia fault, central New Mexico. *U.S. Geological Survey Professional Paper 1440*, 82, 2 plates.

Machette, M. N., Personious, S. F., Kelson, K. I., Haller, K. M., & Dart, R. L. (1998). Map of Quaternary faults and folds in New Mexico and adjacent areas. *USGS Open-file report 98-521*.

Mack, G. H., & Seager, W. R. (1995). Transfer zones in the southern Rio Grande rift. *Journal of the Geological Society*, *152*(3), 551-560.

Manley, C. R., Glazner, A. F., & Farmer, G. L. (2000). Timing of volcanism in the Sierra Nevada of California: Evidence for Pliocene delamination of the batholithic root?. *Geology*, *28*(9), 811-814.

May, S. J., & Russell, L. R. (1994). Thickness of the syn-rift Santa Fe Group in the Albuquerque Basin and its relation to structural style. In Keller, G. R., & Cather, S. M. (Eds.), *Basins of the Rio Grande rift: Structure, stratigraphy, and tectonic setting: Geological Society of America Special Paper 291*, 113-124.

McCall, A. M., & Kodama, K. P. (2014). Anisotropy-based inclination correction for the Moenave Formation and Wingate Sandstone: implications for Colorado Plateau rotation. *Frontiers in Earth Science*, *2*, 15.

McClay, K. R., Dooley, T., Whitehouse, P., & Mills, M. (2002). 4-D evolution of rift systems: Insights from scaled physical models. *AAPG bulletin*, *86*(6), 935-959.

McIntosh, W. C., & Quade J. (1995). ^{40}Ar/^{39}Ar geochronology of the tephra layers in the Santa Fe Group, Española Basin, New Mexico. *New Mexico Geological Society Guidebook, 46th Field Conference*, 279-287.

McMillan, M. E., Angevine, C. L., & Heller, P. L. (2002). Post depositional tilt of the Miocene-Pliocene Ogallala Group on the western Great Plains: Evidence of late Cenozoic uplift of the Rocky Mountains. *Geology, 30*(1), 63–66.

McMillan, N. J., Dickin, A. P., & Haag, D. (2000). Evolution of magma source regions in the Rio Grande rift, southern New Mexico. *GSA Bulletin, 112*(10), 1582-1593.

Miggins, D. P., Thompson, R. A., Pillmore, C. L., Snee, L. W., Stern, C. R. (2002). Extension and uplift of the northern Rio Grande rift: Evidence from $^{40}Ar/^{39}Ar$ geochronology from the Sangre de Cristo Mountains, south-central Colorado and northern New Mexico. In Menzies, M. A., Klemperer, S. L., Ebinger, C. J., Baker, J. (Eds.), *Volcanic Rifted Margins: Geological Society of America Special Paper 362*, 47–64.

Miller, M. G. (1999). Active breaching of a geometric segment boundary in the Sawatch Range normal fault, Colorado, USA. *Journal of Structural Geology, 21*, 769–776.

Minor, S.A., Caine, J.S., Ruleman, C.A., Fridrich, C.J., Chan, C.F., Brandt, T.R., Holm-Denoma, C.S., Morgan, L.E., Cosca, M.A., and Grauch, V.J.S. (2019). Geologic map of the Poncha Pass area, Chaffee, Fremont, and Saguache Counties, Colorado. *U.S. Geological Survey Scientific Investigations Map 3436*, (scale 1:24,000).

Molnar, N, E., Cruden, A. R., & Betts, P. G. (2017). Interactions between propagating rotational rifts and linear rheological heterogeneities: Insights from three-dimensional laboratory experiments. *Tectonics, 36*, 420-443.

Morgan, M. L. (2017). Colorado Earthquake Map Server: http://dnrwebmapgdev.state.co.us/CGSOnline/

Morgan, P. W., Seager, R., & Golombek, M. P., (1986). Cenozoic thermal, mechanical and tectonic evolution of the Rio Grande rift. *Journal of Geophysical Research, 91*, 6263–6276.

Morley, C. K. (1988). Variable extension in lake Tanganyika. *Tectonics*, *7*(4), 785-801.

Morley, C. K., Nelson, R. A., Patton, T. L., & Munn, S. G. (1990). Transfer zones in the East African rift system and their relevance to hydrocarbon exploration in rifts (1). *AAPG Bulletin*, *74*(8), 1234-1253.

Muehlberger, W. R., Belcher, R. C., & Goetz, L. K. (1978). Quaternary faulting in trans-Pecos Texas. *Geology*, *6*(6), 337-340.

Muirhead, J. D., Kattenhorn, S. A., & Le Corvec, N. (2015). Varying styles of magmatic strain accommodation across the East African Rift. *Geochemistry, Geophysics, Geosystems*, *16*(8), 2775-2795.

Muirhead, J. D., Kattenhorn, S. A., Lee, H., Mana, S., Turrin, B. D., Fischer, T. P., Kianji, G., Dindi, E., et al. (2016). Evolution of upper crustal faulting assisted by magmatic volatile release during early-stage continental rift development in the East African Rift. *Geosphere, 12*(6), 1670-1700.

Naeser, C. W., Bryant, B., Kunk, M. J., Kellogg, K., Donelick, R. A., & Perry, W. J. Jr. (2002). Tertiary cooling and tectonic history of the White River uplift, Gore Range, and western Front Range, central Colorado: Evidence from fission-track and ^{39}Ar/^{40}Ar ages. *Geological Society of America Special Papers, 366*, 31-53.

Nakai, J. S., Sheehan, A. F., & Bilek, S. L. (2017). Seismicity of the Rocky Mountains and Rio Grande rift from the Earthscope Transportable Array and CREST temporary seismic networks, 2008–2010. *Journal of Geophysical Research: Solid Earth*, *122*(3), 2173-2192.

Nelson, R. A., Patton, T. L., & Morley, C. K. (1992). Rift-segment interaction and its relation to hydrocarbon exploration in continental rift systems. *American Association of Petroleum Geologists Bulletin, 76*, 1153-1160.

New Mexico Bureau of Geology and Mineral Resources (2003). Geologic Map of New Mexico, (scale 1:500,000).

Nixon, C. W., McNeill, L. C., Bull, J. M., Bell, R. E., Gawthorpe, R. L., Henstock, T. J., ... & Ferentinos, G. (2016). Rapid spatiotemporal variations in rift structure during development of the Corinth Rift, central Greece. *Tectonics*, *35*(5), 1225-1248.

Reiners, P. W., Farley, K. A., & Hickes, H. J. (2002). He diffusion and (U–Th)/He thermochronometry of zircon: initial results from Fish Canyon Tuff and Gold Butte. *Tectonophysics, 349*(1), 297-308.

Reiners, P. W. (2005). Zircon (U-Th)/He thermochronometry. *Reviews in Mineralogy and Geochemistry, 58*(1), 151-179.

Reyners, M., Eberhart-Phillips, D., & Stuart, G. (2007). The role of fluids in lower crustal earthquakes near continental rifts. *Nature*, *446*, 1075-1078.

Ricketts, J. W., Karlstrom, K. E., & Kelley, S. A. (2015). Embryonic core complexes in narrow continental rifts: The importance of low-angle normal faults in the Rio Grande rift of central New Mexico. *Geosphere*, *11*(2), 425-444.

Ricketts, J. W., Kelley, S. A., Karlstrom, K. E., Schmandt, B., Donahue, M. S., & van Wijk, J. (2016). Synchronous opening of the Rio Grande rift along its entire length at 25–10 Ma supported by apatite (U-Th)/He and fission-track thermochronology, and evaluation of possible driving mechanisms. *Geological Society of America Bulletin*, *v. 128*(3-4), 397–424.

Rowland, J. V., Baker, E., Ebinger, C. J., Keir, D., Kidane, T., Biggs, J., ... & Wright, T. J. (2007). Fault growth at a nascent slow-spreading ridge: 2005 Dabbahu rifting episode, Afar. *Geophysical Journal International*, *171*(3), 1226-1246.

Rowland, J. V., Wilson, C. J., & Gravley, D. M. (2010). Spatial and temporal variations in magma-assisted rifting, Taupo Volcanic Zone, New Zealand. *Journal of Volcanology and Geothermal Research*, *190*(1-2), 89-108.

Rudzitis, S., Reid, M. R., & Blichert-Toft, J. (2016). On edge melting under the Colorado Plateau margin. *Geochemistry, Geophysics, Geosystems*, *17*, 2835-2854.

Russell, L. R., & Snelson, S. (1994). Structure and tectonics of the Albuquerque basin segment of the Rio Grande rift: Insights from reflection seismic data. *Geological Society of America, Special Paper*, *291*, 83-112.

Sanford, A. R., Mott, R. P., Shuleski, P. J., Rinehart, E. J., Caravella, F. J., Ward, R. M. & Wallace, T. C. (1977). Geophysical Evidence for a Magma Body in the Crust in the Vicinity of Socorro, New Mexico,. In The Earth's Crust (Eds.) Heacock, J. G., Keller, G.V., Oliver, J. E. & Simmons, G. *American Geophysical Union*, Washington, D.C.

Savage. M.K., Silver, P.G., & Meyer, R.P. (1990). Observations of teleseismic shearwave splitting in the Basin and Range from portable and permanent stations. *Geophysical Research Letters*, *17*, 21-24.

Scott, D. H., & Trask, N. J. (1971). Geology of the lunar crater volcanic field, Nye County, Nevada.

Scott, G. R. (1975). Reconnaissance geologic map of the Buena Vista quadrangle, Chaffee and Park Counties, Colorado. *U.S. Geological Survey, Miscellaneous Field Studies Map MF-657* (scale 1:62,500).

Shannon, J. R. (1988). Geology of the Mount Aetna cauldron complex, Sawatch Range, Colorado. [Doctoral Thesis], Colorado School of Mines, Golden, CO.

Shaw, C. A., & Karlstrom, K. E. (1999). The Yavapai-Mazatzal crustal boundary in the Southern Rocky Mountains. *Rocky Mountain Geology, 34*(1), 37-52.

Shirvell, C., Stockli, D.F., Axen, G.J., & Grove, M. (2009). Miocene–Pliocene exhumation along the West Salton Detachment Fault (WSDF), Southern California, from (U–Th)/He thermochronometry of Apatite and Zircon. *Tectonics, 28*(2).

Shuster, D. L., Flowers, R. M., & Farley, K. A. (2006). The influence of natural radiation damage on helium diffusion kinetics in apatite. *Earth and Planetary Science Letters, 249*(3-4), 148-161.

Smith, G. A. (2004). Middle to late Cenozoic development of the Rio Grande rift and adjacent regions in northern New Mexico. In Mack, G. H., & Giles, K. A. (Eds.), *The geology of New Mexico: A geologic history: New Mexico Geological Society, Special Publication 11*, 331-358.

Stahl, T., & Niemi, N. A. (2017). Late Quaternary faulting in the Sevier Desert driven by magmatism. *Scientific reports*, *7*, 44372.

Stockli, D. F., Farley, K. A., & Dumitru, T. A. (2000). Calibration of the apatite (UTh)/ He thermochronometer on an exhumed fault block, White Mountains, California. *Geology*, *28*(11), 983-986.

Stockli, D. F., Surpless, B. E., Dumitru, T. A., & Farley, K. A. (2002). Thermochronological constraints on the timing and magnitude of Miocene and Pliocene extension in the central Wassuk Range, western Nevada. *Tectonics*, *21*(4).

Taylor, R. B. (1975). Neogene tectonism in south-central Colorado. *Geological Society of America Memoirs*, *144*, 211-226.

Tweto, O. (1979). The Rio Grande rift system in Colorado. In Reiker, R. E., (Ed.), *Rio Grande rift: Tectonics and magmatism*. Washington D.C. American Geophysical Union, 33-56.

U.S. Geological Survey (2006). Quaternary fault and fold database for the United States, accessed February 2018 from USGS web site: http//earthquake.usgs.gov/hazards/qfaults/.

Valentine, G. A., & Cortés, J. A. (2013). Time and space variations in magmatic and phreatomagmatic eruptive processes at Easy Chair (Lunar Crater Volcanic Field, Nevada, USA). *Bulletin of Volcanology*, *75*(9), 752.

Van Alstine, R. E. (1969). Geology and Mineral Deposits of the Poncha Springs NE Quadrangle, Chaffee County, Colorado. *U. S. Geological Survey Special Paper 626*, 1-52.

Van Alstine, R. E., & Lewis, G. E. (1960). Pliocene sediments near Salida, Chaffee County, Colorado. *U.S. Geological Survey Professional Paper 400-B*, B245.

van Wijk, J., Koning, D., Axen, G., Coblentz, D., Gragg, E., & Sion, B. (2018). Tectonic subsidence, geoid analysis, and the Miocene-Pliocene unconformity in the Rio

Grande rift, southwestern United States: Implications for mantle upwelling as a driving force for rift opening. *Geosphere*, *14*(2), 684-709.

van Wijk, J. W., Baldridge, W. S., van Hunen, J., Goes, S., Aster, R., Coblentz, D.D., Grand, S. P., & Ni, J. (2010). Small-scale convection at the edge of the Colorado Plateau: Implications for topography, magmatism, and evolution of Proterozoic Lithosphere. *Geology*, *38*(7), 611–614.

Wilks, M., and Chapin, C. E., 1997, The New Mexico geochronological database: New Mexico Bureau of Mines and Mineral Resources, Digital Database Series, Database DDS–DB1, CDROM.

Woodward, L.A. (1977). Rate of crustal extension across the Rio Grande rift near Albuquerque, New Mexico. *Geology*, *5*, 269-272.

Zhu, L., & Fan, M. (2018). Detrital Zircon Provenance Record of Middle Cenozoic Landscape Evolution in the Southern Rockies, USA. *Sedimentary Geology*.

Zoback, M. L., & Thompson, G. A. (1978). Basin and Range rifting in northern Nevada: Clues from a mid-Miocene rift and its subsequent offsets. *Geology*, *6*(2), 111-116.

Figure 1.

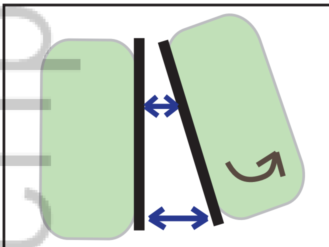	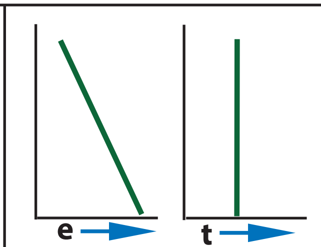	**Rotation** • Synchronous initiation • Rate of extension not diagnostic • Magnitude of extension greater farther from the pole of rotation	**Examples:** Arabian-African Plate and Red Sea rift (Molnar et al., 2017); Colorado Plateau & Rio Grande rift (Brown and Golombeck, 1986; Kreemer et al., 2010)
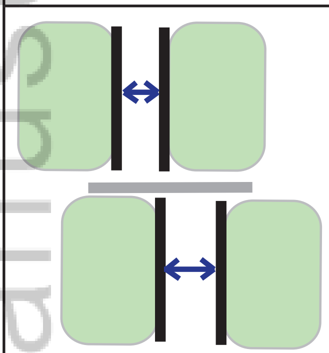	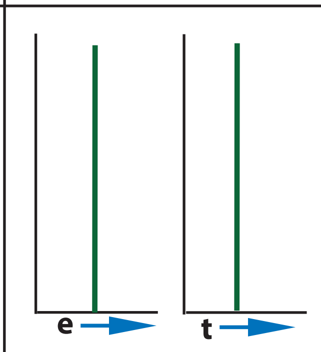	**Oblique extension & transfer on pre-existing weakness** • Synchronous initiation • Rates of extension not diagnostic • Magnitude of extension not diagnostic	**Examples:** Kenya-Ethiopian rifts and Turkana depression (Brune et al., 2017); Malawi rift & Rio Grande rift (Nelson et al., 1992; Ebinger, 1984)
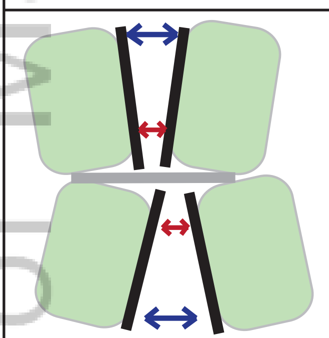	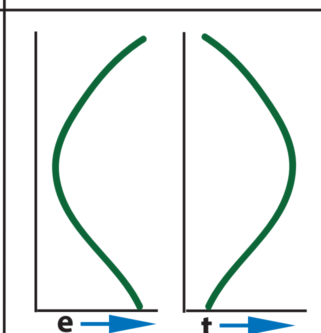	**Fault propagation and linkage on pre-existing weakness** • Asynchronous initiation • Rate of extension not diagnostic • Magnitude of extension greater at t_1 and less at t_2	**Examples:** western rift valley of the East African rift system (Ebinger, 1989; Molnar et al., 2017)
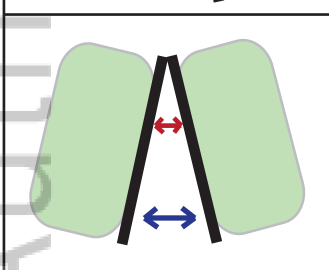	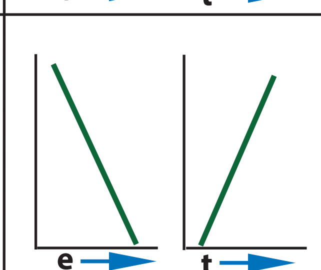	**Rift propagation via hot-spot, plume or magma migration** • Asynchronous initiation • Rate of extension not diagnostic • Magnitude of extension greater at t_1 and less at t_2	**Examples:** Iceland (Lavecchia et al., 2017); Walker Lane Belt (Busby et al., 2013)
	extension magnitude initiation time		

Figure 2.

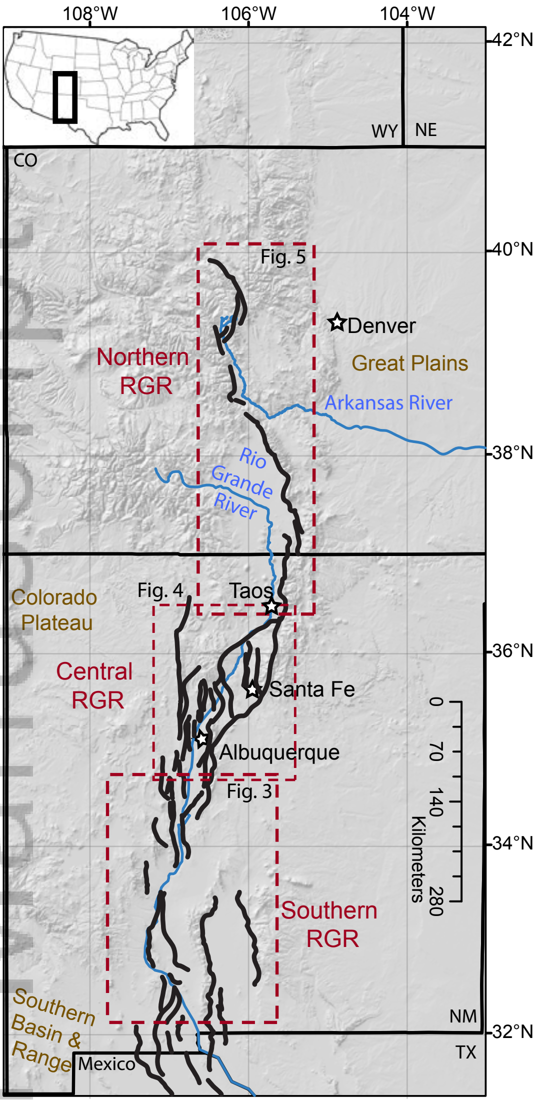
108°W
106°W
104°W
42°N
40°N
38°N
36°N
34°N
32°N
WY
NE
CO
Fig. 5
Denver
Great Plains
Northern
RGR
Arkansas River
Rio
Grande
River
Colorado
Plateau
Fig. 4
Taos
Central
RGR
Santa Fe
Albuquerque
Fig. 3
0
70
140
280
Kilometers
Southern
RGR
Southern
Basin &
Range
Mexico
NM
TX

Figure 3.

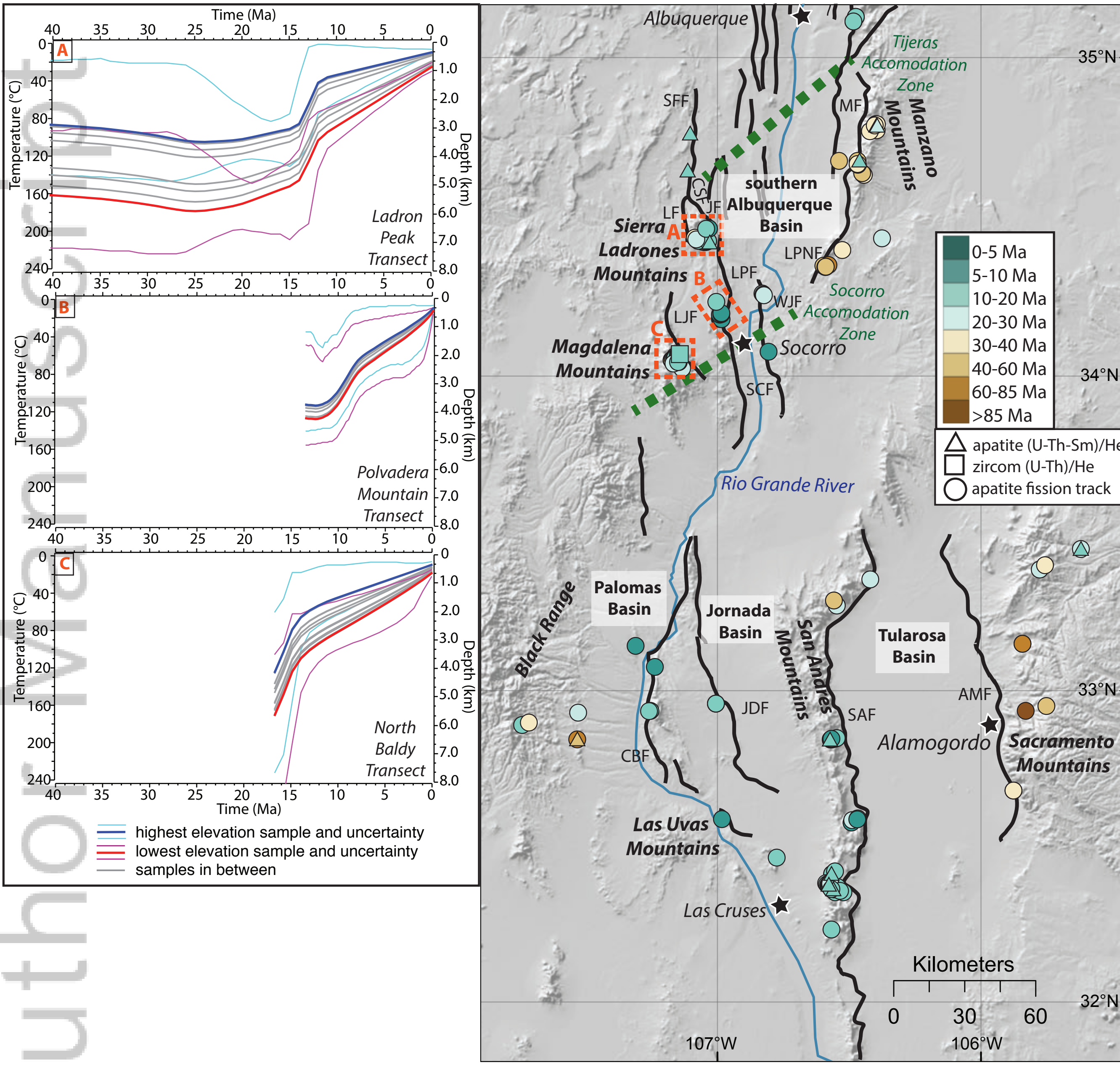
Time (Ma)
40 35 30 25 20 15 10 5 0
A
Temperature (°C)
Depth (km)
Ladron Peak Transect
B
Polvadera Mountain Transect
C
North Baldy Transect
Time (Ma)
highest elevation sample and uncertainty
lowest elevation sample and uncertainty
samples in between
Albuquerque
Tijeras Accomodation Zone
35°N
SFF
MF
Manzano Mountains
CSF
JF
southern Albuquerque Basin
LF
Sierra Ladrones Mountains
LPNF
LPF
WJF
Socorro Accomodation Zone
LJF
Magdalena Mountains
Socorro
SCF
34°N
0-5 Ma
5-10 Ma
10-20 Ma
20-30 Ma
30-40 Ma
40-60 Ma
60-85 Ma
>85 Ma
apatite (U-Th-Sm)/He
zircom (U-Th)/He
apatite fission track
Rio Grande River
Palomas Basin
Black Range
Jornada Basin
San Andres Mountains
Tularosa Basin
33°N
AMF
JDF
SAF
CBF
Alamogordo
Sacramento Mountains
Las Uvas Mountains
Las Cruses
Kilometers
0 30 60
32°N
107°W
106°W

Figure 4.

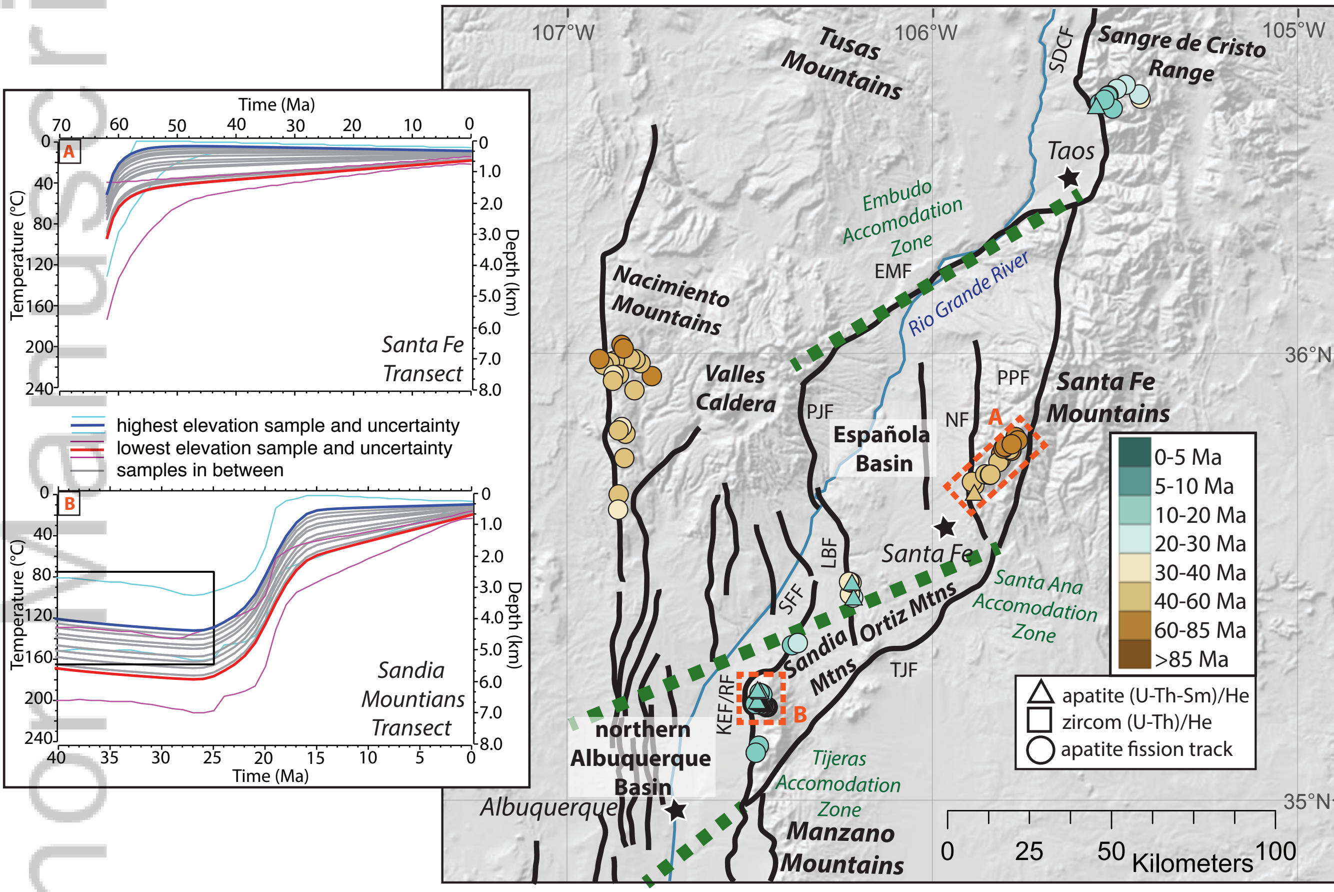

Time (Ma)
70 60 50 40 30 20 10 0
A
Temperature (°C)
Depth (km)
Santa Fe Transect
highest elevation sample and uncertainty
lowest elevation sample and uncertainty
samples in between
B
Sandia Mountians Transect
40 35 30 25 20 15 10 5 0
Time (Ma)
107°W
106°W
105°W
36°N
35°N
Tusas Mountains
Sangre de Cristo Range
SDCF
Taos
Embudo Accomodation Zone
EMF
Rio Grande River
Nacimiento Mountains
Valles Caldera
PJF
PPF
NF
Santa Fe Mountains
Española Basin
Santa Fe
LBF
SFF
Santa Ana Accomodation Zone
Sandia Mtns
Ortiz Mtns
TJF
KEF/RF
northern Albuquerque Basin
Albuquerque
Tijeras Accomodation Zone
Manzano Mountains
0-5 Ma
5-10 Ma
10-20 Ma
20-30 Ma
30-40 Ma
40-60 Ma
60-85 Ma
>85 Ma
apatite (U-Th-Sm)/He
zircom (U-Th)/He
apatite fission track
0 25 50 Kilometers 100

Figure 5.

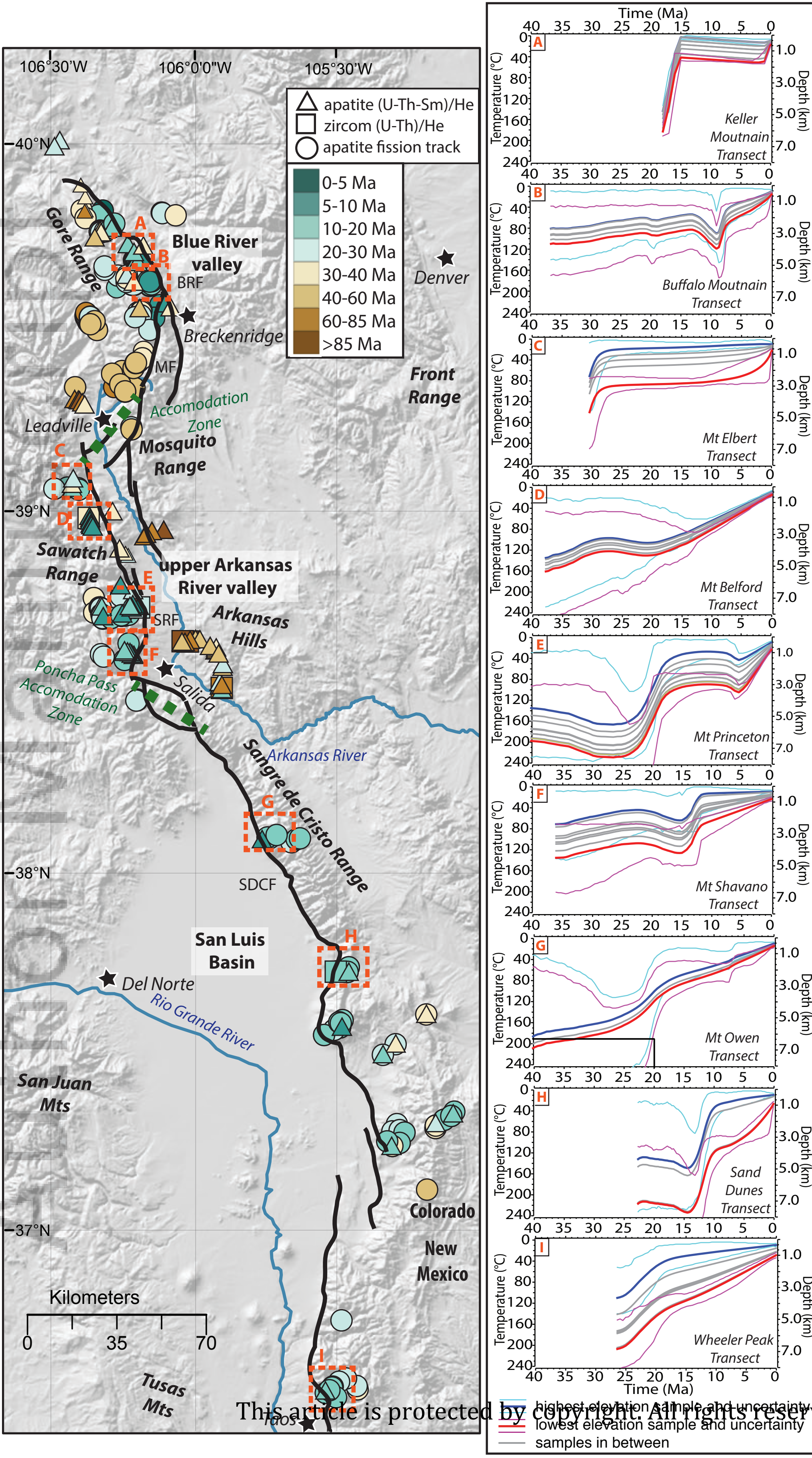

106°30'W
106°0'0"W
105°30'W
40°N
39°N
38°N
37°N
apatite (U-Th-Sm)/He
zircom (U-Th)/He
apatite fission track
0-5 Ma
5-10 Ma
10-20 Ma
20-30 Ma
30-40 Ma
40-60 Ma
60-85 Ma
>85 Ma
Gore Range
Blue River valley
BRF
Breckenridge
Denver
MF
Accomodation Zone
Leadville
Mosquito Range
Front Range
Sawatch Range
upper Arkansas River valley
Arkansas Hills
SRF
Poncha Pass Accomodation Zone
Salida
Arkansas River
Sangre de Cristo Range
SDCF
San Luis Basin
Del Norte
Rio Grande River
San Juan Mts
Colorado
New Mexico
Kilometers
0
35
70
Tusas Mts
Taos
Time (Ma)
Temperature (°C)
Depth (km)
Keller Moutnain Transect
Buffalo Moutnain Transect
Mt Elbert Transect
Mt Belford Transect
Mt Princeton Transect
Mt Shavano Transect
Mt Owen Transect
Sand Dunes Transect
Wheeler Peak Transect
highest elevation sample and uncertainty
lowest elevation sample and uncertainty
samples in between

Figure 6.

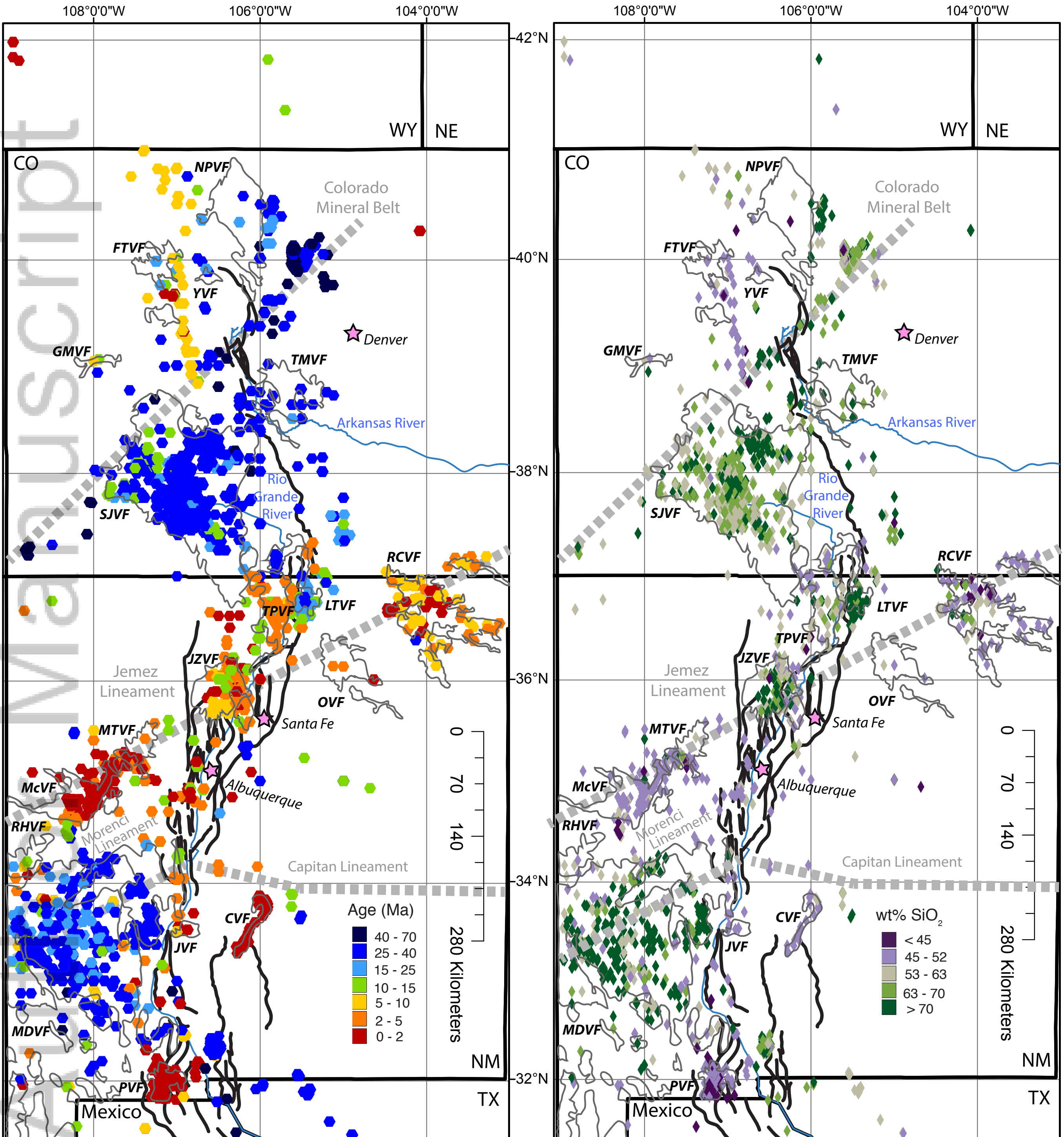
108°0'0"W
106°0'0"W
104°0'0"W
42°N
40°N
38°N
36°N
34°N
32°N
WY
NE
CO
NM
TX
Mexico
NPVF
FTVF
YVF
GMVF
TMVF
SJVF
RCVF
LTVF
TPVF
JZVF
OVF
MTVF
McVF
RHVF
CVF
JVF
MDVF
PVF
Colorado Mineral Belt
Denver
Arkansas River
Rio Grande River
Jemez Lineament
Santa Fe
Albuquerque
Morenci Lineament
Capitan Lineament
Age (Ma)
40 - 70
25 - 40
15 - 25
10 - 15
5 - 10
2 - 5
0 - 2
wt% SiO_2
< 45
45 - 52
53 - 63
63 - 70
> 70
0
70
140
280 Kilometers

Figure 7.

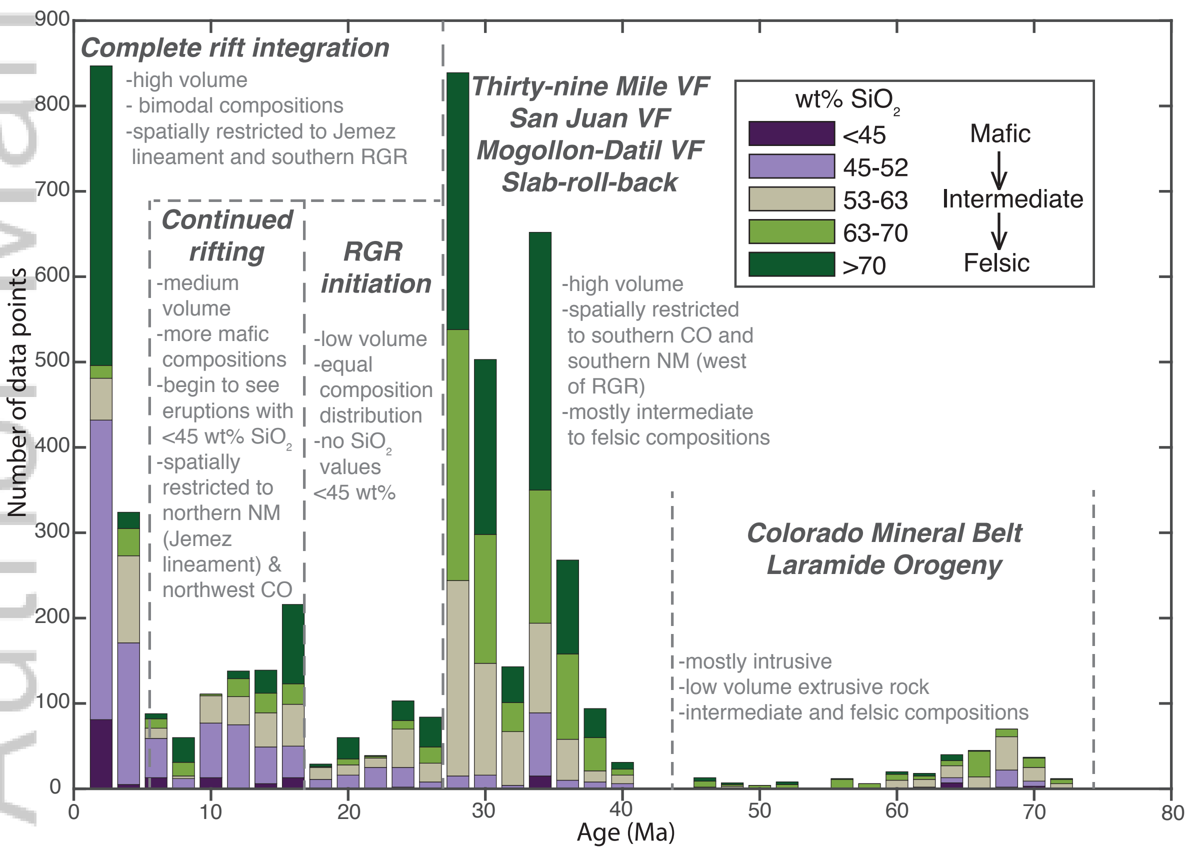

Number of data points
900
800
700
600
500
400
300
200
100
0
0
10
20
30
40
50
60
70
80
Age (Ma)
Complete rift integration
-high volume
- bimodal compositions
-spatially restricted to Jemez lineament and southern RGR
Continued rifting
-medium volume
-more mafic compositions
-begin to see eruptions with <45 wt% SiO2
-spatially restricted to northern NM (Jemez lineament) & northwest CO
RGR initiation
-low volume
-equal composition distribution
-no SiO2 values <45 wt%
Thirty-nine Mile VF
San Juan VF
Mogollon-Datil VF
Slab-roll-back
-high volume
-spatially restricted to southern CO and southern NM (west of RGR)
-mostly intermediate to felsic compositions
wt% SiO2
<45
45-52
53-63
63-70
>70
Mafic
Intermediate
Felsic
Colorado Mineral Belt
Laramide Orogeny
-mostly intrusive
-low volume extrusive rock
-intermediate and felsic compositions

Figure 8.

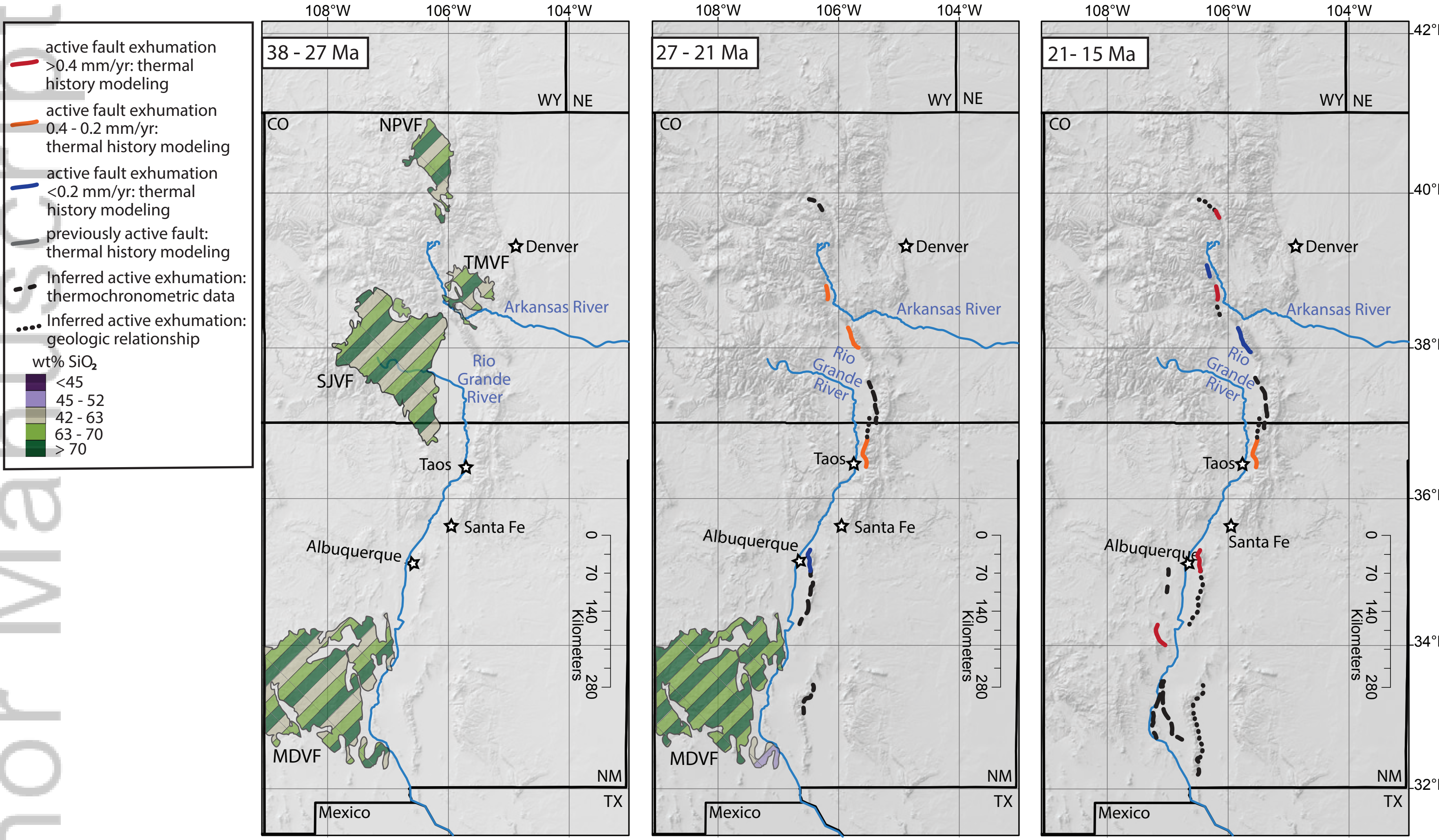

active fault exhumation >0.4 mm/yr: thermal history modeling
active fault exhumation 0.4 - 0.2 mm/yr: thermal history modeling
active fault exhumation <0.2 mm/yr: thermal history modeling
previously active fault: thermal history modeling
Inferred active exhumation: thermochronometric data
Inferred active exhumation: geologic relationship
wt% SiO_2
<45
45 - 52
42 - 63
63 - 70
> 70
38 - 27 Ma
27 - 21 Ma
21- 15 Ma
108°W
106°W
104°W
42°N
40°N
38°N
36°N
34°N
32°N
WY
NE
CO
NM
TX
Mexico
NPVF
TMVF
SJVF
MDVF
Denver
Arkansas River
Rio Grande River
Taos
Santa Fe
Albuquerque
0
70
140
280
Kilometers

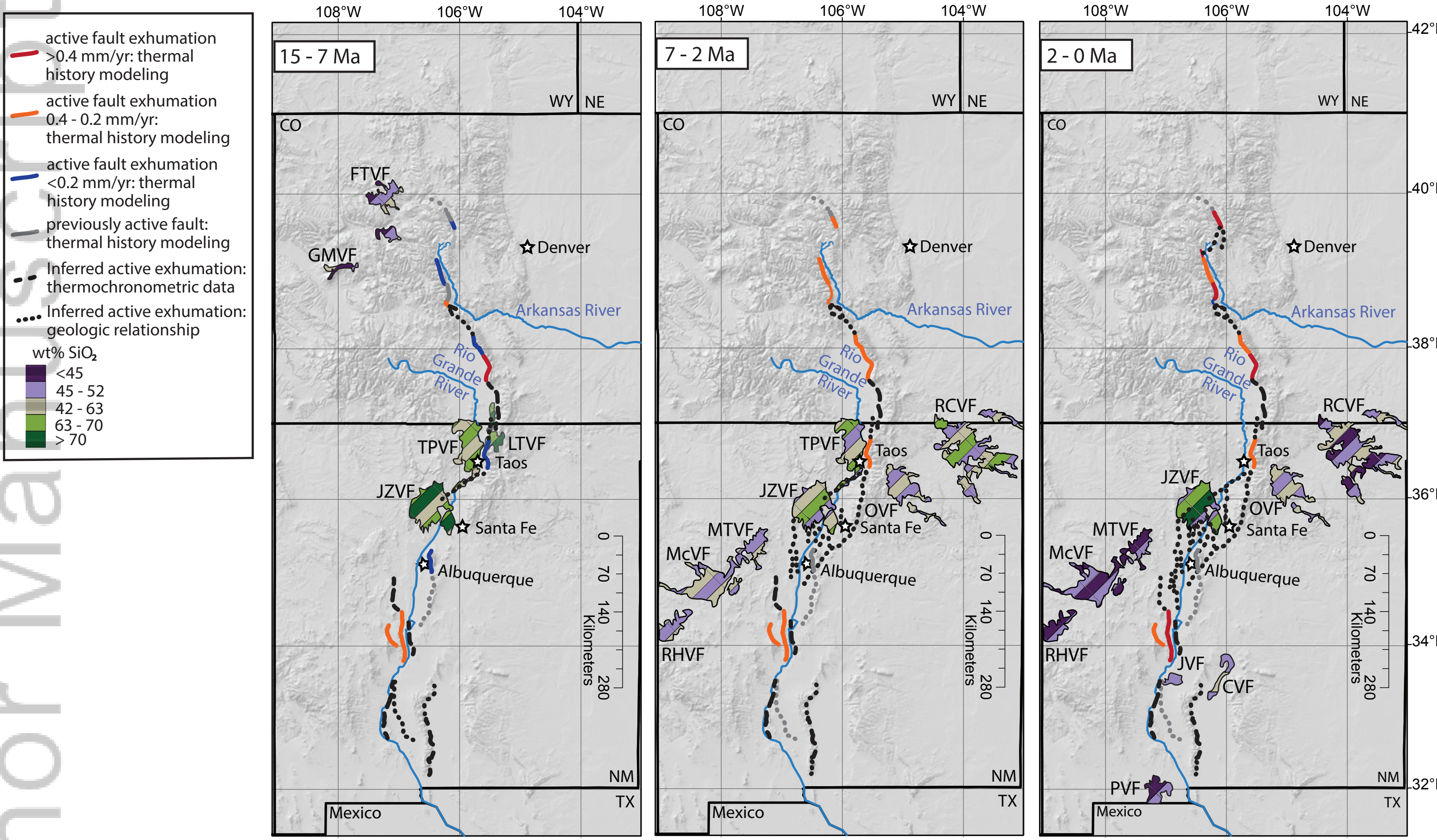

active fault exhumation >0.4 mm/yr: thermal history modeling
active fault exhumation 0.4 - 0.2 mm/yr: thermal history modeling
active fault exhumation <0.2 mm/yr: thermal history modeling
previously active fault: thermal history modeling
Inferred active exhumation: thermochronometric data
Inferred active exhumation: geologic relationship
wt% SiO_2
<45
45 - 52
42 - 63
63 - 70
> 70
15 - 7 Ma
7 - 2 Ma
2 - 0 Ma
108°W
106°W
104°W
42°N
40°N
38°N
36°N
34°N
32°N
WY
NE
CO
NM
TX
Mexico
Denver
Arkansas River
Rio Grande River
Taos
Santa Fe
Albuquerque
FTVF
GMVF
TPVF
LTVF
JZVF
RCVF
OVF
MTVF
McVF
RHVF
JVF
CVF
PVF
0
70
140
280
Kilometers

Figure 9.

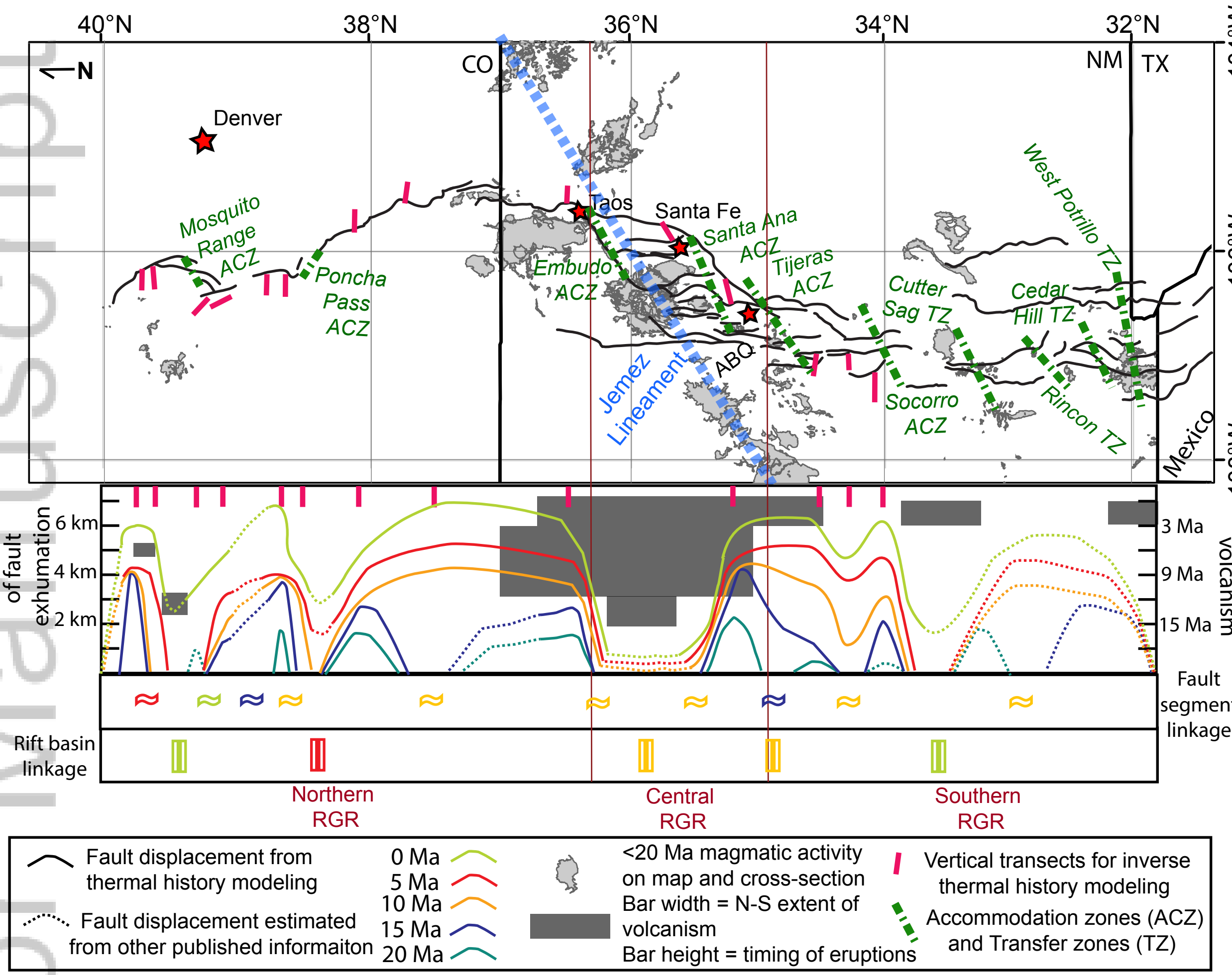

40°N
38°N
36°N
34°N
32°N
104°W
106°W
108°W
N
Denver
CO
NM
TX
Mexico
Taos
Santa Fe
ABQ
Mosquito Range ACZ
Poncha Pass ACZ
Embudo ACZ
Santa Ana ACZ
Tijeras ACZ
Cutter Sag TZ
Socorro ACZ
Cedar Hill TZ
Rincon TZ
West Potrillo TZ
Jemez Lineament
magnitude of fault exhumation
6 km
4 km
2 km
3 Ma
9 Ma
15 Ma
Age of volcanism
Fault segment linkage
Rift basin linkage
Northern RGR
Central RGR
Southern RGR
Fault displacement from thermal history modeling
Fault displacement estimated from other published informaiton
0 Ma
5 Ma
10 Ma
15 Ma
20 Ma
<20 Ma magmatic activity on map and cross-section
Bar width = N-S extent of volcanism
Bar height = timing of eruptions
Vertical transects for inverse thermal history modeling
Accommodation zones (ACZ) and Transfer zones (TZ)

Figure 10.

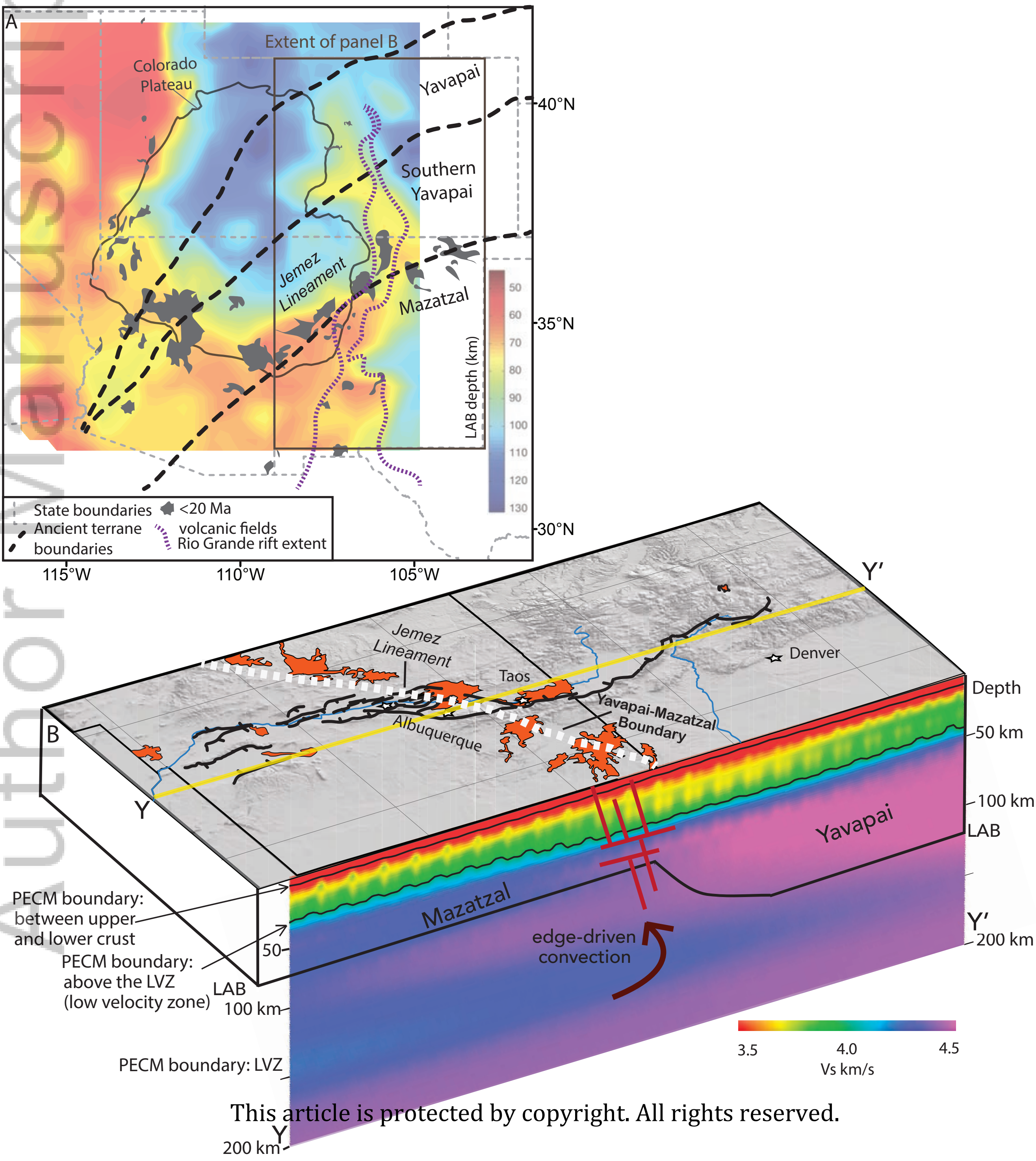

A
Extent of panel B
Colorado Plateau
Yavapai
Southern Yavapai
Jemez Lineament
Mazatzal
LAB depth (km)
50
60
70
80
90
100
110
120
130
40°N
35°N
30°N
115°W
110°W
105°W
State boundaries
Ancient terrane boundaries
<20 Ma volcanic fields
Rio Grande rift extent
B
Jemez Lineament
Taos
Denver
Albuquerque
Yavapai-Mazatzal Boundary
Y
Y′
Depth
50 km
100 km
LAB
200 km
Yavapai
Mazatzal
edge-driven convection
PECM boundary: between upper and lower crust
PECM boundary: above the LVZ (low velocity zone)
PECM boundary: LVZ
50
LAB
100 km
200 km
3.5
4.0
4.5
Vs km/s

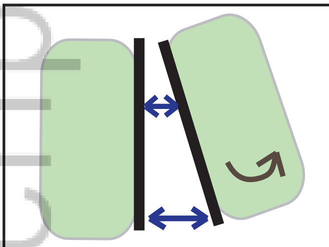	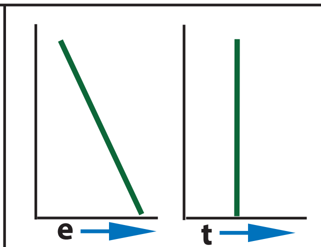	**Rotation** • Synchronous initiation • Rate of extension not diagnostic • Magnitude of extension greater farther from the pole of rotation	**Examples:** Arabian-African Plate and Red Sea rift (Molnar et al., 2017); Colorado Plateau & Rio Grande rift (Brown and Golombeck, 1986; Kreemer et al., 2010)
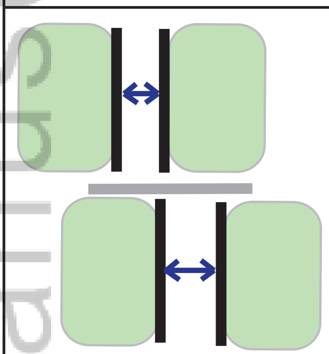	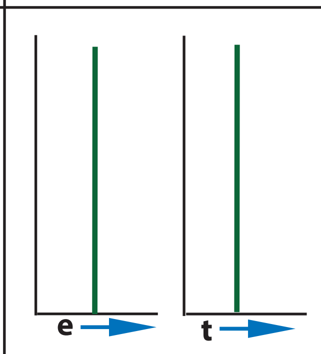	**Oblique extension & transfer on pre-existing weakness** • Synchronous initiation • Rates of extension not diagnostic • Magnitude of extension not diagnostic	**Examples:** Kenya-Ethiopian rifts and Turkana depression (Brune et al., 2017); Malawi rift & Rio Grande rift (Nelson et al., 1992; Ebinger, 1984)
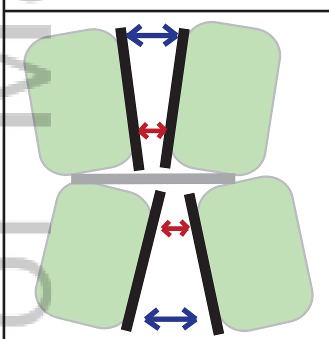	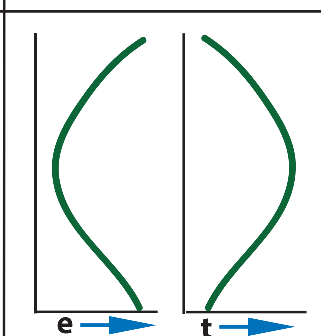	**Fault propagation and linkage on pre-existing weakness** • Asynchronous initiation • Rate of extension not diagnostic • Magnitude of extension greater at t_1 and less at t_2	**Examples:** western rift valley of the East African rift system (Ebinger, 1989; Molnar et al., 2017)
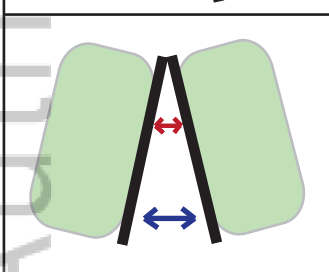	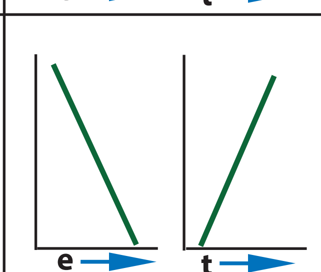	**Rift propagation via hot-spot, plume or magma migration** • Asynchronous initiation • Rate of extension not diagnostic • Magnitude of extension greater at t_1 and less at t_2	**Examples:** Iceland (Lavecchia et al., 2017); Walker Lane Belt (Busby et al., 2013)
↔ t_1 ↔ t_2	extension magnitude / initiation time		

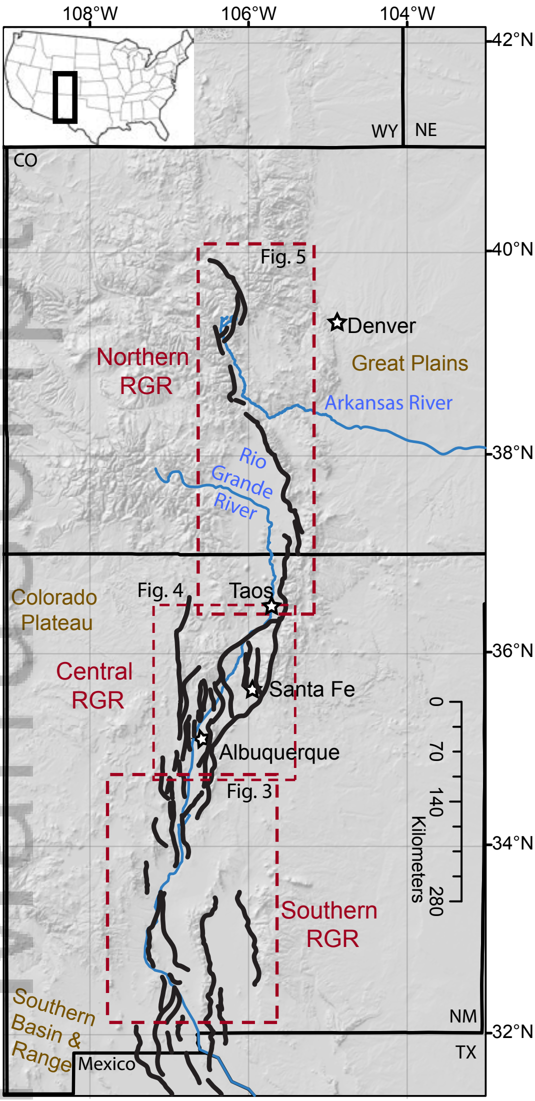
108°W
106°W
104°W
42°N
40°N
38°N
36°N
34°N
32°N
WY
NE
CO
Fig. 5
Denver
Great Plains
Northern
RGR
Arkansas River
Rio
Grande
River
Colorado
Plateau
Fig. 4
Taos
Central
RGR
Santa Fe
Albuquerque
Fig. 3
0
70
140
280
Kilometers
Southern
RGR
Southern
Basin &
Range
Mexico
NM
TX

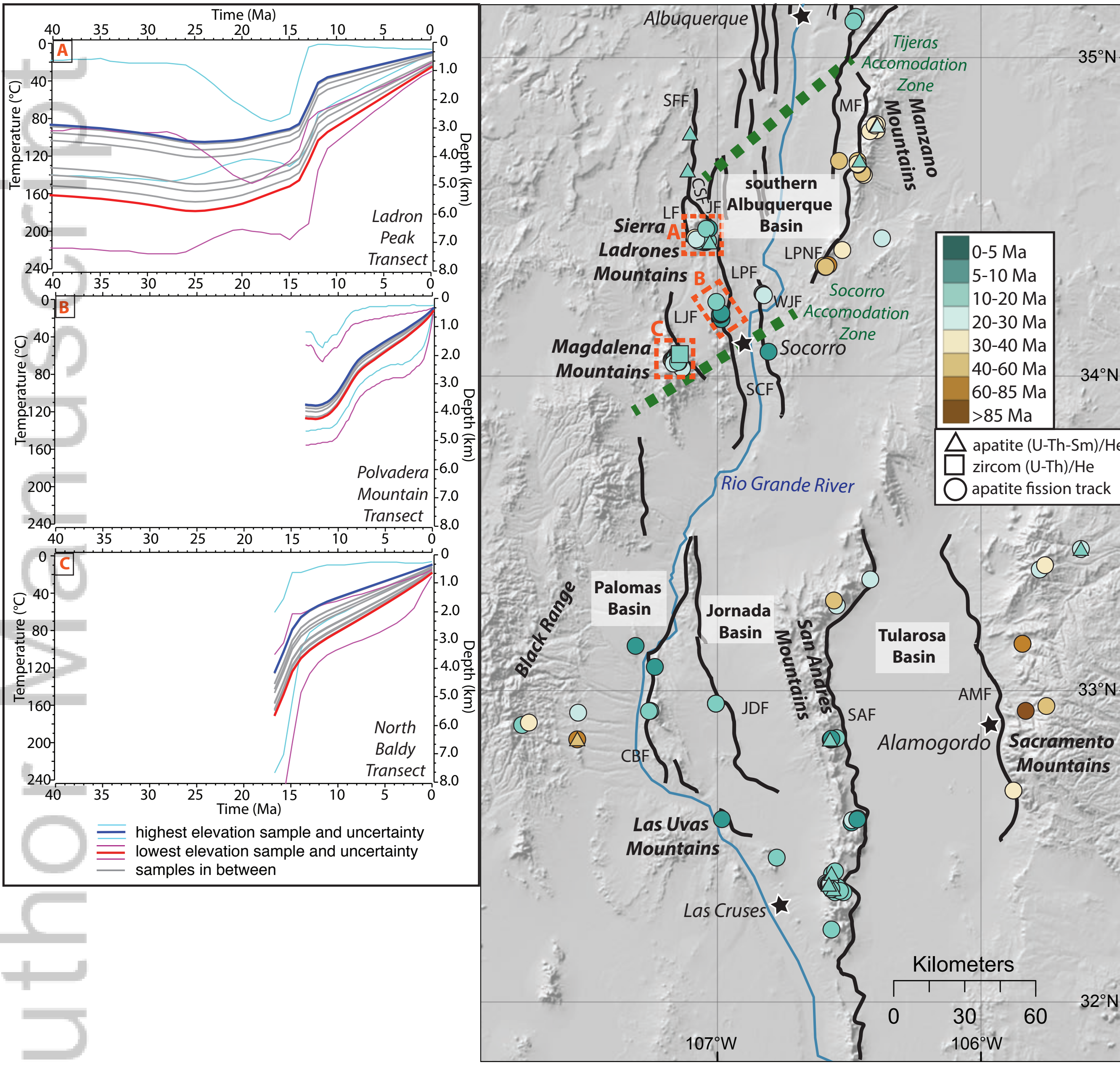

Time (Ma)
A
Ladron Peak Transect
B
Polvadera Mountain Transect
C
North Baldy Transect
Temperature (°C)
Depth (km)
highest elevation sample and uncertainty
lowest elevation sample and uncertainty
samples in between
Albuquerque
Tijeras Accomodation Zone
35°N
SFF
MF
Manzano Mountains
southern Albuquerque Basin
CS
JF
LF
Sierra Ladrones Mountains
LPNF
LPF
Socorro Accomodation Zone
WJF
LJF
Magdalena Mountains
Socorro
34°N
SCF
0-5 Ma
5-10 Ma
10-20 Ma
20-30 Ma
30-40 Ma
40-60 Ma
60-85 Ma
>85 Ma
apatite (U-Th-Sm)/He
zircom (U-Th)/He
apatite fission track
Rio Grande River
Black Range
Palomas Basin
Jornada Basin
San Andres Mountains
Tularosa Basin
AMF
33°N
JDF
SAF
Alamogordo
Sacramento Mountains
CBF
Las Uvas Mountains
Las Cruses
Kilometers
0
30
60
32°N
107°W
106°W

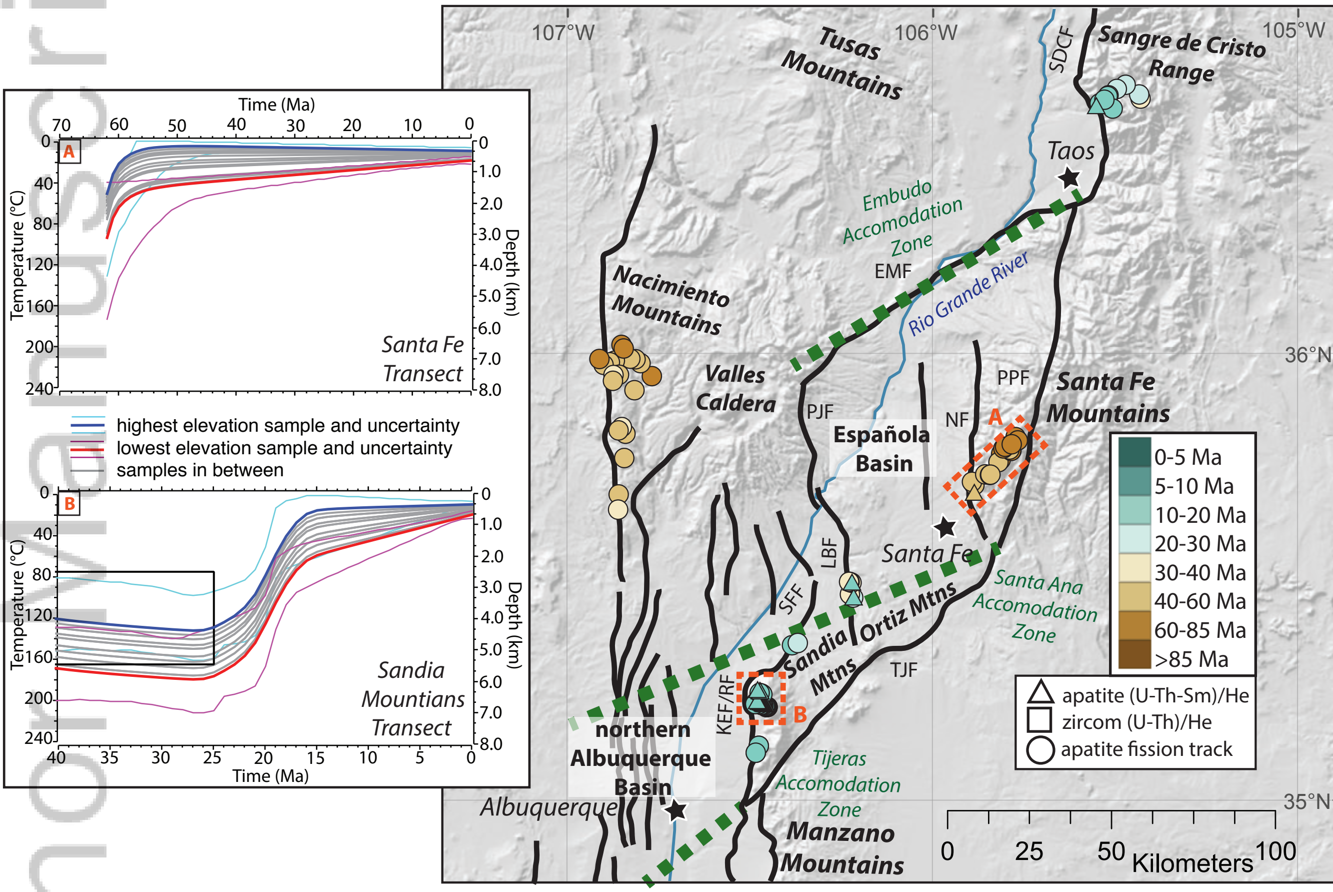
Time (Ma)
70 60 50 40 30 20 10 0
A
Temperature (°C)
Depth (km)
Santa Fe Transect
highest elevation sample and uncertainty
lowest elevation sample and uncertainty
samples in between
B
Sandia Mountians Transect
Time (Ma)
40 35 30 25 20 15 10 5 0
107°W
106°W
105°W
36°N
35°N
Tusas Mountains
Sangre de Cristo Range
SDCF
Taos
Embudo Accomodation Zone
EMF
Rio Grande River
Nacimiento Mountains
Valles Caldera
PJF
Española Basin
NF
PPF
Santa Fe Mountains
Santa Fe
LBF
SFF
Santa Ana Accomodation Zone
Sandia Mtns
Ortiz Mtns
TJF
KEF/RF
northern Albuquerque Basin
Albuquerque
Tijeras Accomodation Zone
Manzano Mountains
0-5 Ma
5-10 Ma
10-20 Ma
20-30 Ma
30-40 Ma
40-60 Ma
60-85 Ma
>85 Ma
apatite (U-Th-Sm)/He
zircom (U-Th)/He
apatite fission track
0 25 50 100
Kilometers

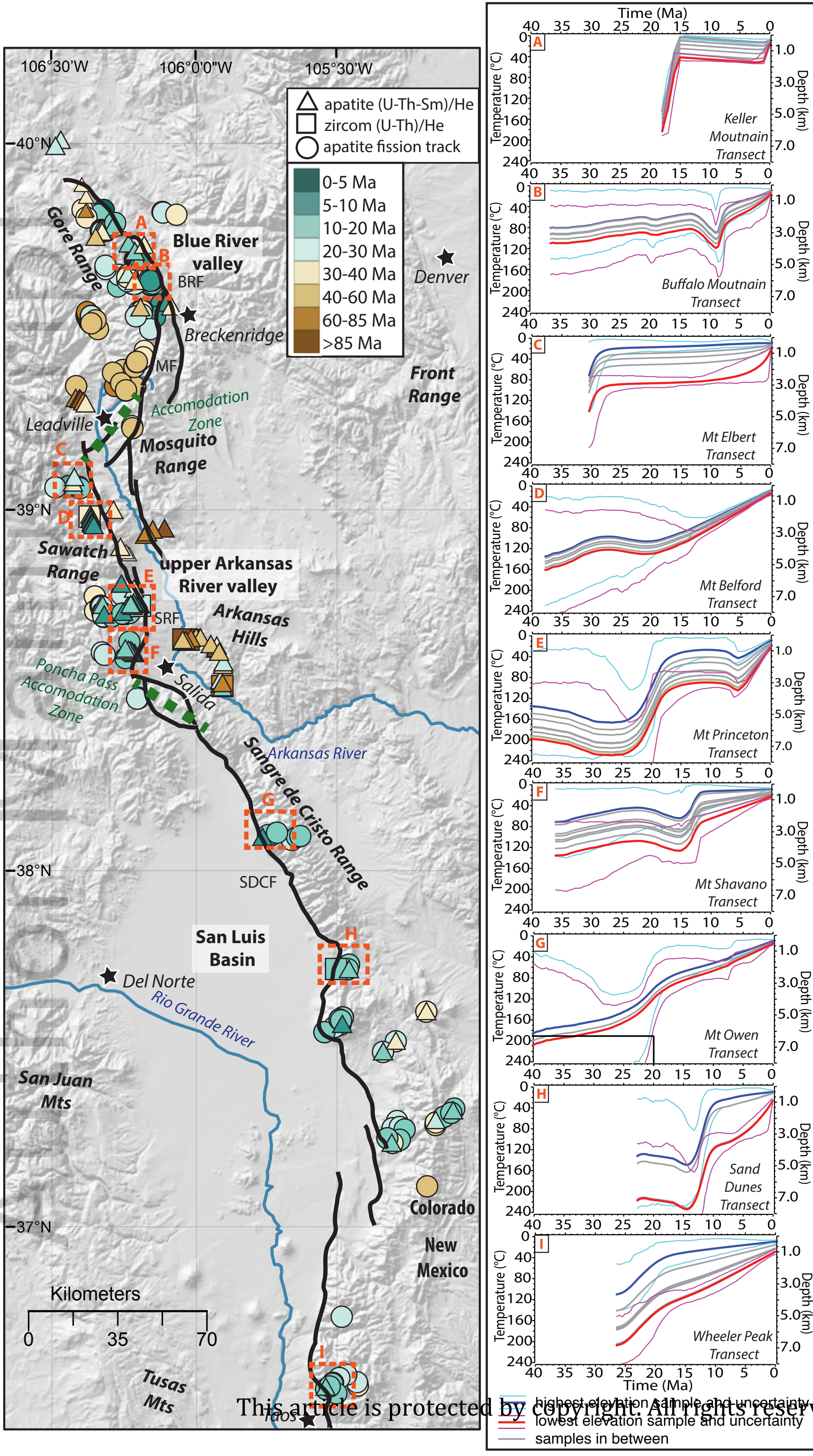

apatite (U-Th-Sm)/He
zircom (U-Th)/He
apatite fission track
0-5 Ma
5-10 Ma
10-20 Ma
20-30 Ma
30-40 Ma
40-60 Ma
60-85 Ma
>85 Ma
106°30'W
106°0'0"W
105°30'W
40°N
39°N
38°N
37°N
Gore Range
Blue River valley
BRF
Breckenridge
MF
Denver
Front Range
Leadville
Accomodation Zone
Mosquito Range
Sawatch Range
upper Arkansas River valley
Arkansas Hills
SRF
Poncha Pass Accomodation Zone
Salida
Arkansas River
Sangre de Cristo Range
SDCF
San Luis Basin
Del Norte
Rio Grande River
San Juan Mts
Colorado
New Mexico
Kilometers
0
35
70
Tusas Mts
Taos
Time (Ma)
Temperature (°C)
Depth (km)
Keller Moutnain Transect
Buffalo Moutnain Transect
Mt Elbert Transect
Mt Belford Transect
Mt Princeton Transect
Mt Shavano Transect
Mt Owen Transect
Sand Dunes Transect
Wheeler Peak Transect
highest elevation sample and uncertainty
lowest elevation sample and uncertainty
samples in between

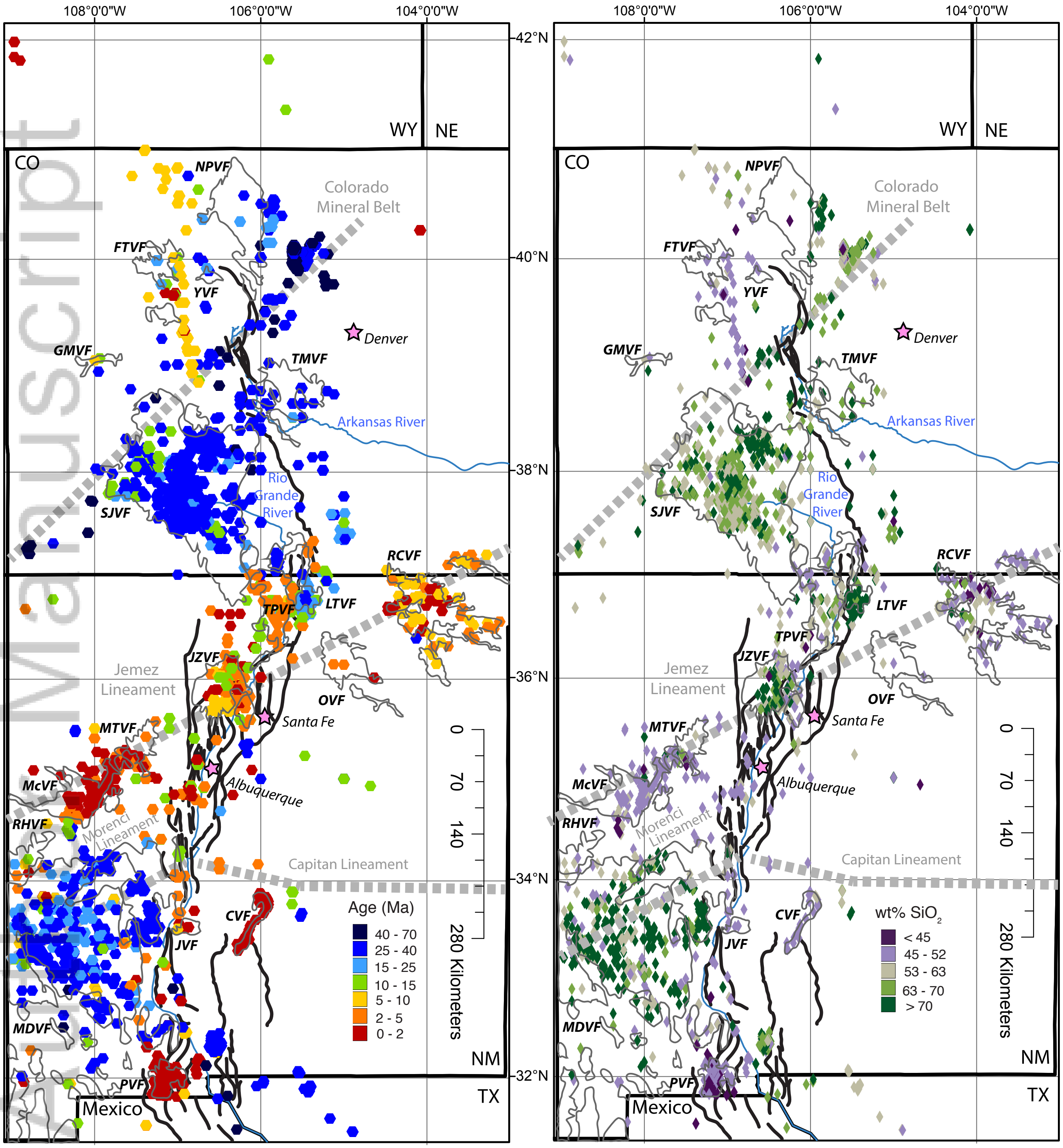

108°0'0"W
106°0'0"W
104°0'0"W
42°N
40°N
38°N
36°N
34°N
32°N
WY
NE
CO
NM
TX
Mexico
NPVF
FTVF
YVF
GMVF
TMVF
SJVF
RCVF
LTVF
TPVF
JZVF
OVF
MTVF
McVF
RHVF
CVF
JVF
MDVF
PVF
Colorado Mineral Belt
Denver
Arkansas River
Rio Grande River
Jemez Lineament
Santa Fe
Albuquerque
Morenci Lineament
Capitan Lineament
Age (Ma)
40 - 70
25 - 40
15 - 25
10 - 15
5 - 10
2 - 5
0 - 2
wt% SiO2
< 45
45 - 52
53 - 63
63 - 70
> 70
0
70
140
280 Kilometers

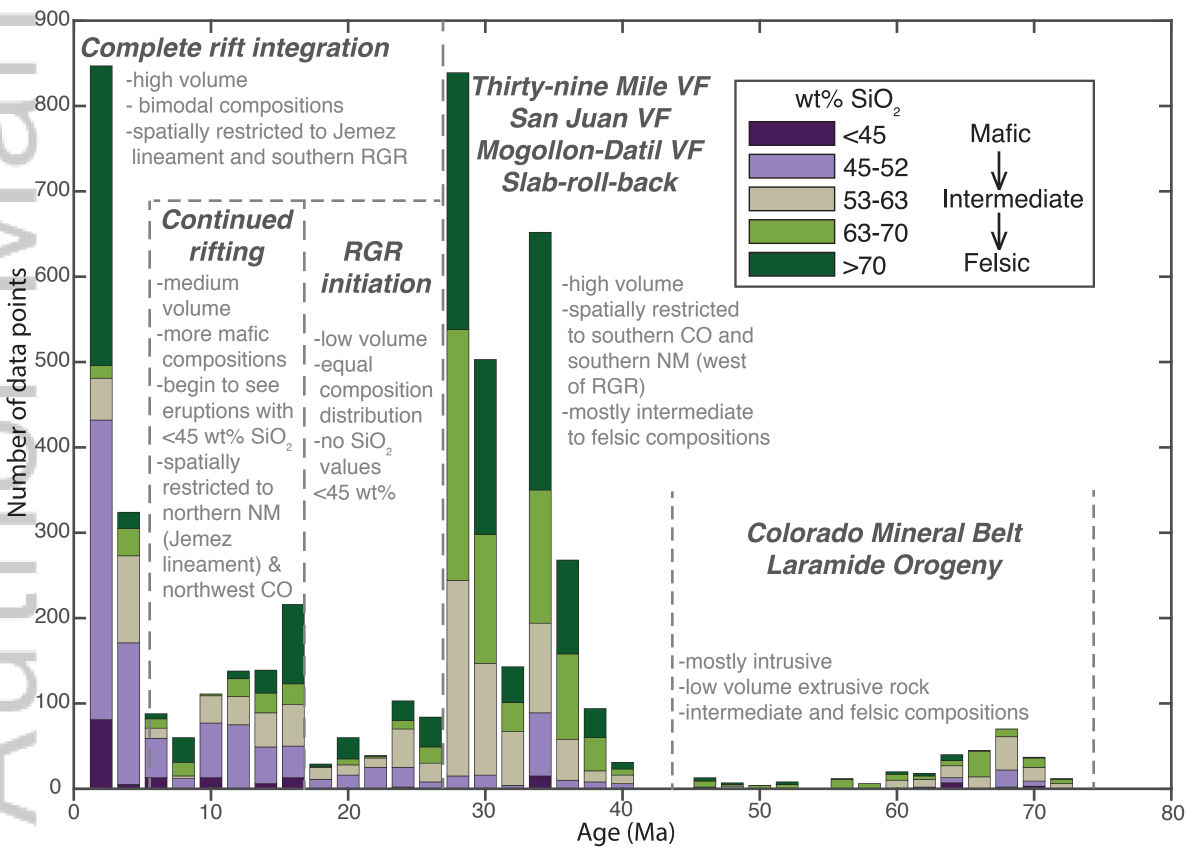
Complete rift integration
-high volume
- bimodal compositions
-spatially restricted to Jemez lineament and southern RGR
Continued rifting
-medium volume
-more mafic compositions
-begin to see eruptions with <45 wt% SiO2
-spatially restricted to northern NM (Jemez lineament) & northwest CO
RGR initiation
-low volume
-equal composition distribution
-no SiO2 values <45 wt%
Thirty-nine Mile VF
San Juan VF
Mogollon-Datil VF
Slab-roll-back
-high volume
-spatially restricted to southern CO and southern NM (west of RGR)
-mostly intermediate to felsic compositions
wt% SiO2
<45
45-52
53-63
63-70
>70
Mafic
Intermediate
Felsic
Colorado Mineral Belt
Laramide Orogeny
-mostly intrusive
-low volume extrusive rock
-intermediate and felsic compositions
Number of data points
Age (Ma)
0
100
200
300
400
500
600
700
800
900
10
20
30
40
50
60
70
80

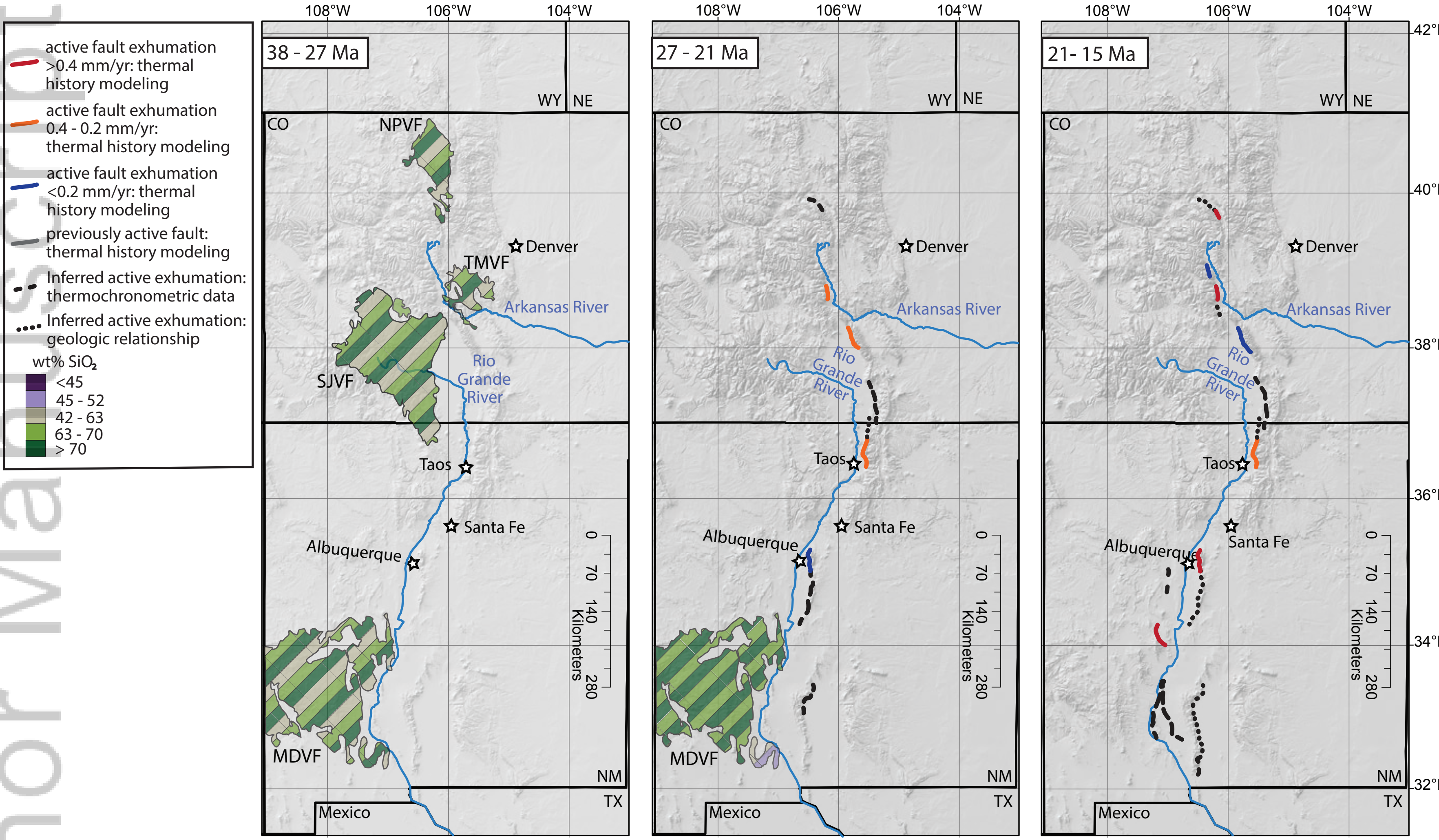

active fault exhumation >0.4 mm/yr: thermal history modeling
active fault exhumation 0.4 - 0.2 mm/yr: thermal history modeling
active fault exhumation <0.2 mm/yr: thermal history modeling
previously active fault: thermal history modeling
Inferred active exhumation: thermochronometric data
Inferred active exhumation: geologic relationship
wt% SiO2
<45
45 - 52
42 - 63
63 - 70
> 70
38 - 27 Ma
27 - 21 Ma
21- 15 Ma
108°W
106°W
104°W
42°N
40°N
38°N
36°N
34°N
32°N
WY
NE
CO
NM
TX
Mexico
NPVF
TMVF
SJVF
MDVF
Denver
Arkansas River
Rio Grande River
Taos
Santa Fe
Albuquerque
0
70
140
280
Kilometers

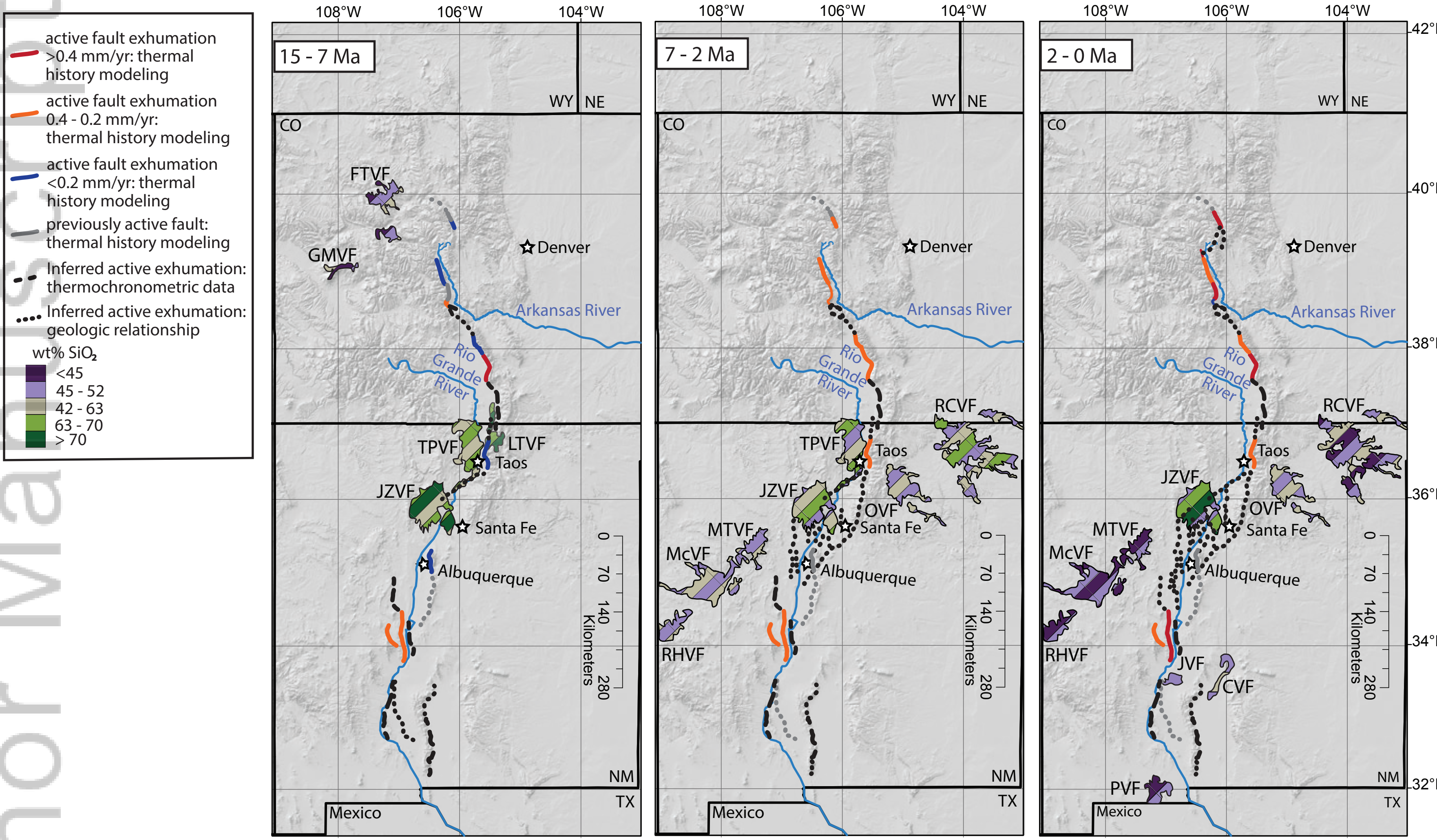
active fault exhumation >0.4 mm/yr: thermal history modeling
active fault exhumation 0.4 - 0.2 mm/yr: thermal history modeling
active fault exhumation <0.2 mm/yr: thermal history modeling
previously active fault: thermal history modeling
Inferred active exhumation: thermochronometric data
Inferred active exhumation: geologic relationship
wt% SiO2
<45
45 - 52
42 - 63
63 - 70
> 70
15 - 7 Ma
7 - 2 Ma
2 - 0 Ma
108°W
106°W
104°W
42°N
40°N
38°N
36°N
34°N
32°N
WY
NE
CO
NM
TX
Mexico
FTVF
GMVF
Denver
Arkansas River
Rio Grande River
TPVF
LTVF
Taos
JZVF
Santa Fe
Albuquerque
RCVF
OVF
MTVF
McVF
RHVF
JVF
CVF
PVF
0
70
140
280
Kilometers

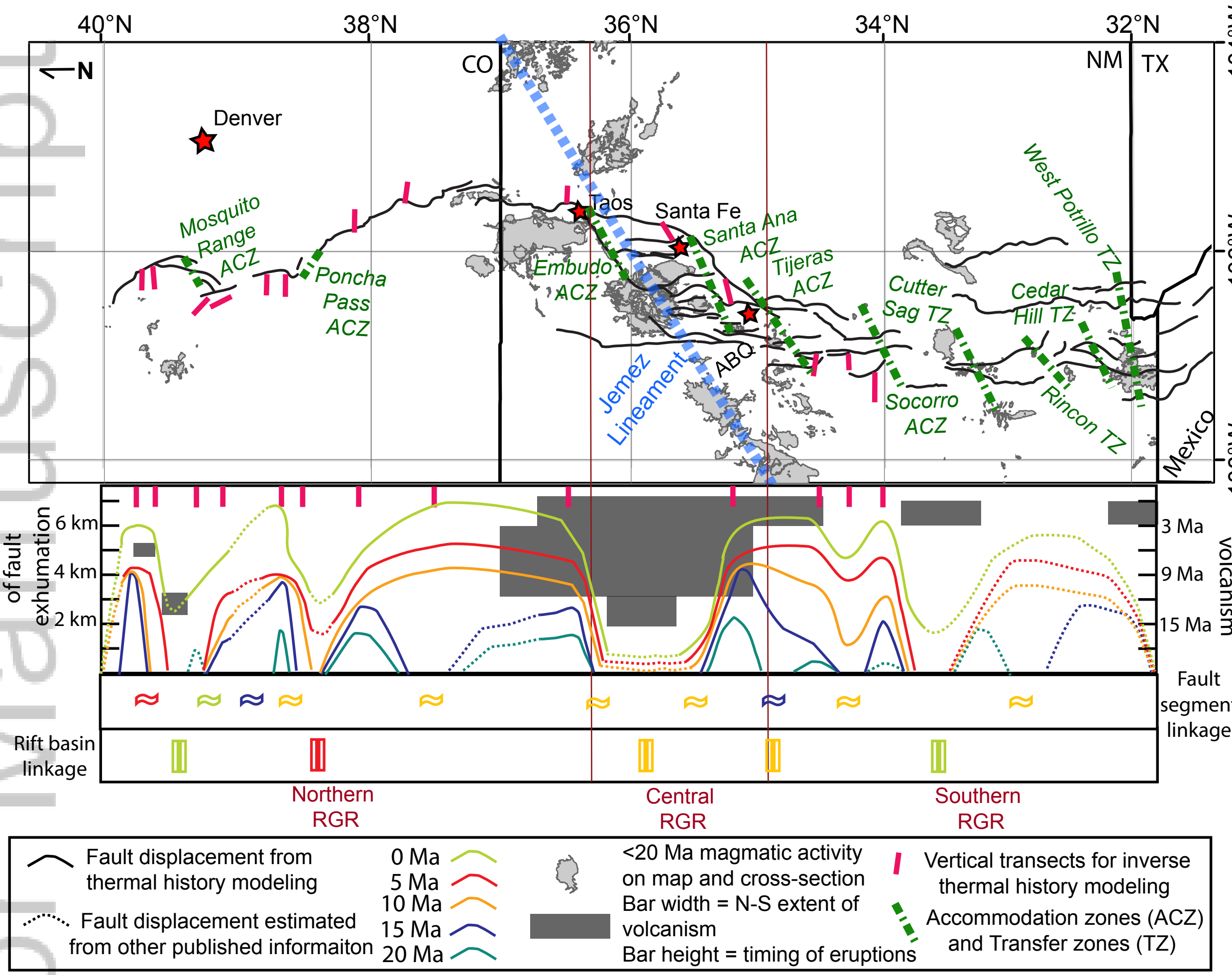

40°N
38°N
36°N
34°N
32°N
104°W
106°W
108°W
N
Denver
CO
NM
TX
Mexico
Taos
Santa Fe
ABQ
Mosquito Range ACZ
Poncha Pass ACZ
Embudo ACZ
Santa Ana ACZ
Tijeras ACZ
Cutter Sag TZ
Socorro ACZ
Cedar Hill TZ
West Potrillo TZ
Rincon TZ
Jemez Lineament
magnitude of fault exhumation
6 km
4 km
2 km
3 Ma
9 Ma
15 Ma
Age of volcanism
Fault segment linkage
Rift basin linkage
Northern RGR
Central RGR
Southern RGR
Fault displacement from thermal history modeling
Fault displacement estimated from other published informaiton
0 Ma
5 Ma
10 Ma
15 Ma
20 Ma
<20 Ma magmatic activity on map and cross-section
Bar width = N-S extent of volcanism
Bar height = timing of eruptions
Vertical transects for inverse thermal history modeling
Accommodation zones (ACZ) and Transfer zones (TZ)

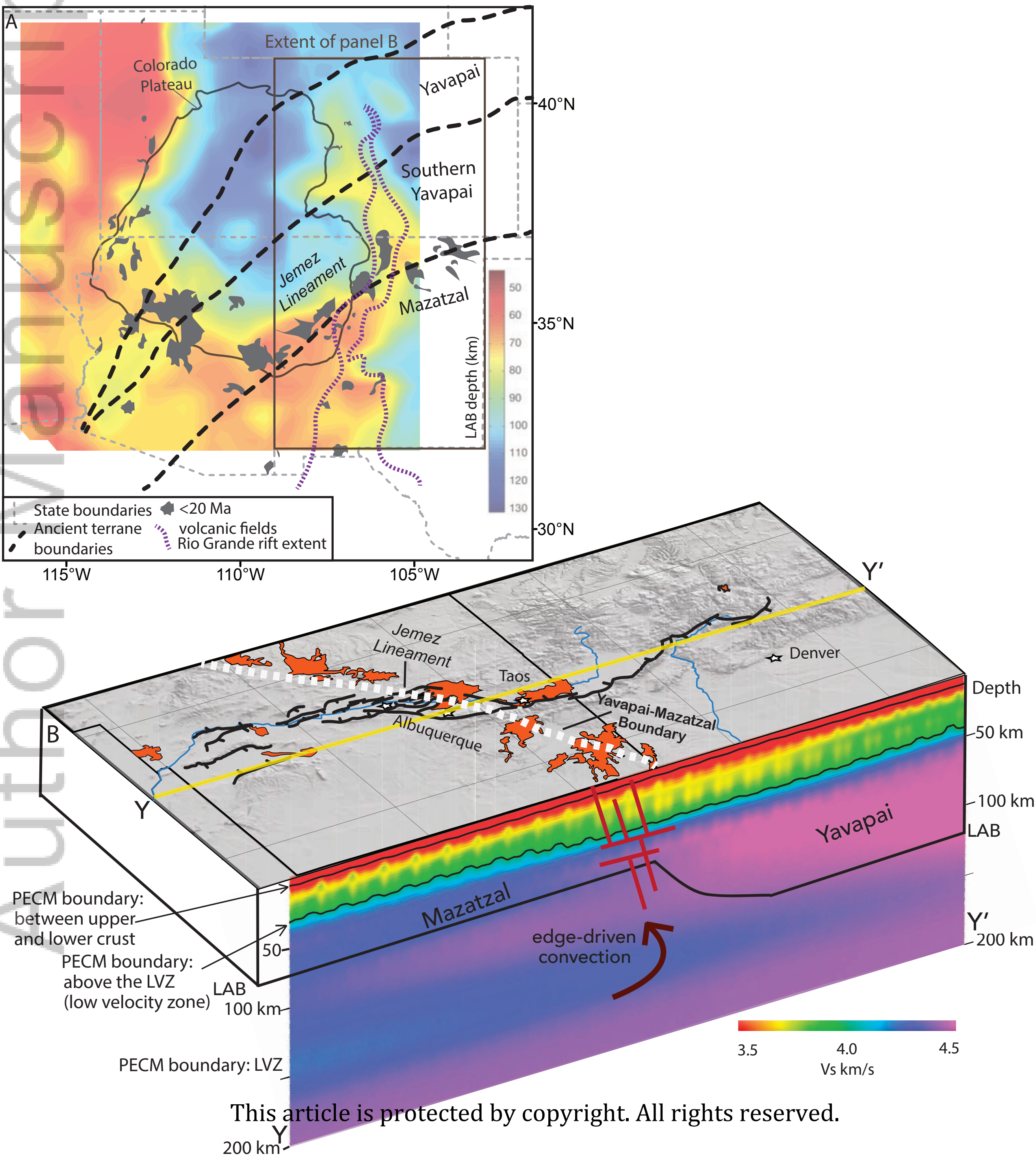
A
Extent of panel B
Colorado
Plateau
Yavapai
Southern
Yavapai
Jemez
Lineament
Mazatzal
LAB depth (km)
50
60
70
80
90
100
110
120
130
40°N
35°N
30°N
115°W
110°W
105°W
State boundaries
Ancient terrane
boundaries
<20 Ma
volcanic fields
Rio Grande rift extent
B
Jemez
Lineament
Taos
Denver
Albuquerque
Yavapai-Mazatzal
Boundary
Y
Y'
Depth
50 km
100 km
LAB
Yavapai
Mazatzal
edge-driven
convection
200 km
PECM boundary:
between upper
and lower crust
PECM boundary:
above the LVZ
(low velocity zone)
LAB
50
100 km
PECM boundary: LVZ
200 km
3.5
4.0
4.5
Vs km/s